# University Review

2008
Vol.2, No.1

## physical engineering of materials

**Alexander Dubček University of Trenčín**

**Izhevsk State Technical University**

Alexander Dubček University of Trenčín

# University Review


Alexander Dubček University of Trenčín


Izhevsk State Technical University

Publishing House:
Alexander Dubček University of Trenčín

University Review

(The international scientific journal founded by two universities from Slovak Republic and Russian Federation)

This journal originated with kindly support of Ministry of Education of the Slovak Republic

## Editorial Office

Študentská 1, 911 50 Trenčín, Tel.: 032/7 400 279, 032/7 400 277
dubovska@tnuni.sk, bodorova@tnuni.sk

## Honorary Editors



## Editor-in-Chief



## Science Editor



## Members

**Redaction**

Bodorová Janka, Mgr.

**Publishing House**

Alexander Dubček University of Trenčín, Študentská 2, 911 50 Trenčín

**Graphic Design**

3z SOLUTIONS - Zuzana Slezáková, www.3zs.sk

**Technical Information**



University Review, Vol. 2, No. 1
Trenčín: Alexander Dubček University of Trenčín
2008, 64 p.
ISSN 1337-6047

# CONTENTS

# CONTRIBUTORS

**Z. Jonšta, VŠB – Technical University of Ostrava, Czech Republic**
e-mail: zdenek.jonsta@vsb.cz
**M. Tvrdý, P. Jonšta, V. Vodárek**

**S. Isic, Faculty of Mechanical Engineering, Mostar, Bosnia and Herzegovina**
e-mail: safet.isic@unmo.ba
**V. Dolecek, Faculty of Mechanical Engineering, Sarajevo, Bosnia and Herzegovina**
e-mail: vldolecek@yahoo.com
**I. Karabegovic, Technical Faculty Bihac, Bosnia and Herzegovina**
e-mail: isak1910@hotmail.com

**Y. Ludwig, S. Mrotzek**
**D. Hülsenberg, Technische Universität Ilmenau, Germany**
e-mail: dagmar.huelsenberg@tu-ilmenau.de

**I. Furár, V. Trnovcová, Faculty of Materials Science and Technology, Slovak University of Technology, Trnava, Slovakia**
e-mail: ivan.furar@stuba.sk
**M. Kadlečíková, Faculty of Electro-engineering and Informatics, Bratislava, Slovakia,**
**J. Pedlíková, Institute of Inorganic Chemistry, Academy of Sciences of Czech Republic, Prague, Czech Republic**

**L. Čížek, M. Tvrdý, VŠB - Technical University of Ostrava, Ostrava**
e-mail: lubomir.cizek@vsb.cz
**S. Król, S. Szulc, R. Bański, Politechnical University of Opole, Opole, Poland**
e-mail: deankrol@po.opole.pl
**A. Hernas**
e-mail: adam.hernasl@polsl.pl

**Z. Češpíro, P. Mossóczy, Czech Technical University, Faculty of Mechanical Engineering, Department of Production Machines and Mechanisms; Prague, Czech Republic**
e-mail: Zdenek.Cespiro@fs.cvut.cz
e-mail: Pavel.Mossoczy@fs.cvut.cz

# CONTRIBUTORS

**J. Kraxner, R. Klement, M. Liška**
**Vitrum Laugaricio – Joint Glass Center of the Institute of Inorganic Chemistry Slovak Academy of Sciences, Alexander Dubček University of Trenčín, and RONA, Trenčín, Slovak Republic**
e-mail: kraxner@centrum.sk
e-mail: klement@tnuni.sk
e-mail: liska@tnuni.sk

**J. Šperl, J. Trčková, Institute of Rock Structure and Mechanics, Prague, Czech Republic**
e-mail: sperl@irsm.cas.cz
e-mail: trckova@irsm.cas.cz

**R. Holušová , J. Borkala, Vítkovice Testing Center,s.r.o., Ostrava, Czech Republic**
e-mail: radka.holusova@vitkovice.cz
e-mail: jiri.borkala@vitkovice.cz

**A. Bjelanović, Faculty of Civil Engineering; Rijeka, Croatia**
e-mail: adriana.bjelanovic@gradri.hr
**V. Pavlić, student of Faculty of Civil Engineering; Rijeka, Croatia**
e-mail: vedran.pavlic@gmail.hr
**V. Rajčić, Faculty of Civil Engineering; Zagreb, Croatia**
e-mail: vrajcic@grad.hr

**J. Běhal, Aeronautical Research and Test Institute, Prague, Czech Republic**
e-mail: behal.jr@vzlu.cz
**N. Ganev, Czech Technical University in Prague, Czech Republic**
e-mail: ganev@troja.fjfi.cvut.cz
**M. Černý, Technometra Radotín, Prague, Czech Republic**
e-mail: cerny@technometra.cz

## Reviewers

**Prof. RNDr. Pavol Koštial, PhD.**
**Prof. Ing. Ivan Letko, PhD.**
**Prof. RNDr. Juraj Slabeycius, PhD.**
**Prof. Ing. Miroslav Kopecký, PhD.**
**Prof. Ing. Ján Vavro, PhD.**
**Prof. RNDr. Ignác Capek, DrSc.**
**Prof. Ing. Eugen Jóna, DrSc.**
**Prof. Ing. Vendelín Macho, DrSc.**
**Prof. Ing. Martin Jambrich, DrSc.**
**Prof. Ing. Ján Štefánik, PhD.**

# RECTOR´S FOREWORD

Assoc. prof. Ing. Miroslav Mečár, PhD.

Dear readers, the issue of the journal you are reading in its English version is a result of a collaboration between Alexander Dubcek University of Trencin and the Izhevsk State University of Technology. This issue No 4 of the second volume is devoted to the research results achieved by researchers and teachers at the Faculty of Industrial Technologies seated in Puchov and by their counterparts at the Izhevsk University.

New management at both universities promotes and supports the forms of cooperation and publishing the research results. Both parties will attempt to publish their research results on equal scale. We would like to inform the academic staff and the public about the activities that are done at both universities so that they can assist the people involved to find the most effective forms of working on mutual projects and collaboration what can help us concentrate on necessary capacity needed for large international projects. We believe that we will succeed in these projects and we will be able to publish their results in the English version of our journal.

I believe that you, our readers, enjoy reading the authors digest and their thoughts shall encourage you in your future career in the field of research and in our future collaboration.

# STRUCTURAL-PHASE ANALYSIS OF CAST NICKEL SUPER-ALLOY INCONEL 792-5A

Z. Jonšta, P. Jonšta, V. Vodárek, M. Tvrdý

## Abstract

The submitted paper deals with analysis of physical-metallurgical characteristics of cast variant of nickel alloy based on INCONEL, namely type IN 792-5A. This variant of nickel super-alloy represents higher type of these alloys thanks to higher contents of cobalt and tantalum. Metallographic analysis of investigated type of nickel super-alloy in as-cast condition contributes to précising of existing notions about possibilities of optimisation of initial state by subsequent heat treatment. The analysis itself is based on evaluation of microstructure in as-cast condition by use of light microscopy and also of more detailed electron microscopy investigation, including chemical micro-analysis. Electron microscopy investigation was performed with use of scanning electron microscope JEOL JSM – 5510 with application of secondary electrons mode. Chemical micro-analysis was made on electron micro-analyser JCX 733, which is equipped with energy dispersive analyser EDX – Sappirs. Conventionally verified etching technique used for preparation of metallographic samples of nickel super-alloys or high-alloyed austenitic Cr-Ni based steels was used for selective analysis of detected phases.

## Key words

nickel super-alloy, as-cast condition, structural-phase analysis

Nickel super-alloys are very often used for structural parts of turbo-blowers. This is caused by the fact that requirements to material for these appliances are extremely high, such as heat resistance at high temperatures, resistance to fatigue failure, resistance to aggressive effect of flue gases, etc. Materials must ensure high operational reliability and safety during exploitation at high temperatures. That's why particularly nickel super-alloys belong to advanced materials, which can fulfil these requirements. Blades are the most expensive part of this equipment, therefore the biggest attention is paid to their service life [1].

Long-time service life and reliability of such equipment during operation at high temperatures is inseparably linked to microstructure or to its stability at long-term high-temperature exposition. One of the types of nickel super-alloys used for these appliances is the INCONEL family of super-alloys. It is cast material that is alloyed in a complex manner on the basis of Cr-Al-Mo-Ti-Nb-Zr [2].

The submitted work analysed cast alloy INCONEL 792-5A, which represents higher type of these alloys due to its higher contents of Co and Ta.

Evaluation is based on assessment of microstructure in as cast condition by light microscopy, and on more detailed analysis performed by electron microscopy, including chemical micro-analysis.

## EXPERIMENTAL MATERIAL

Experimental investigation was made with use of castings manufactured from commercially produced nickel super-alloy INCONEL 792 – 5A. Chemical composition of this super-alloy is given in the Tab. 1 [3].

Tab. 1: Chemical composition of nickel super-alloy INCONEL 792-5A (mass %)

| C | Mn(max) | Si(max) | Cr | Ti | Al | Fe(max) | B |
|---|---|---|---|---|---|---|---|
| 0.06-0.10 | 0.15 | 0.20 | 12.0-13.0 | 3.85-4.50 | 3.15-3.60 | 0.50 | 0.010-0.020 |

| Nb | Ta | Mo | W | Cu(max) | Co(max) | P(max) | S(max) | Ni |
|---|---|---|---|---|---|---|---|---|
| 0.50 | 3.85-4.50 | 1.65-2.15 | 4.50 | 0.50 | 8.50-9.50 | 0.015 | 0.015 | rest |

Complex analysis also specifies zirconium contents in the nickel super-alloy INCONEL 792 – 5A, namely Zr 0.01 – 0,05 mass %.

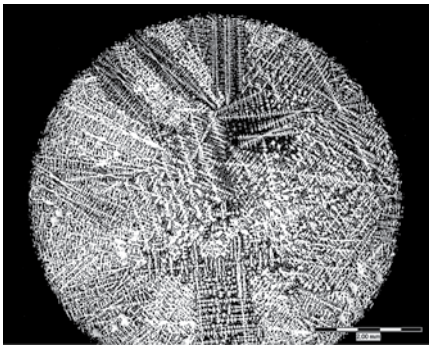

Fig. 1: Basic microstructure of nickel super-alloy INCONEL 792-5A

## DESCRIPTION OF RESULTS AND THEIR ANALYSIS

Fig. 1 shows microstructure of the given type of nickel super-alloy. Fig. 2 documents the given alloy at greater magnification.

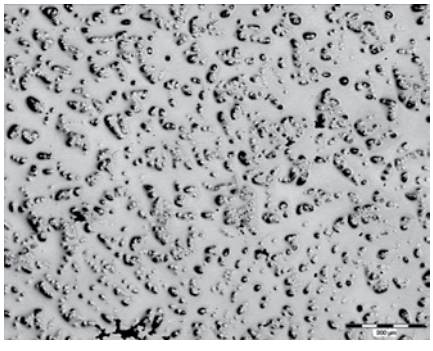

Fig. 2: Microstructure of nickel super-alloy INCONEL 792-5A

Properties of grain boundaries are obvious from the photo shown in the Fig. 3. It is apparent that precipitates are in preference segregated along grain boundaries and their concentration is evidently lower in volume of grains. Obtaining of more detailed overview would require more detailed analysis performed with use of electron microscopy.

In case of the given nickel super-alloy IN 792 – 5A particles of carbides of Ta and Ti were detected in basic metallic matrix, which represents type MX. These particles were observed particularly in inter-dendritic areas. Characteristic pictures expressed by reflected electrons are shown in the Fig. 4a, b.

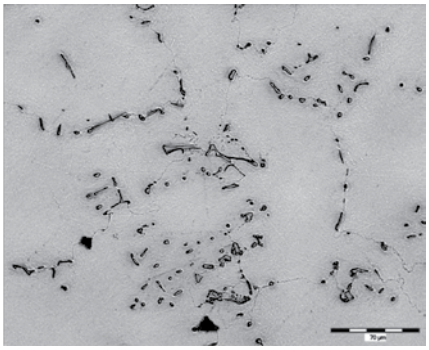

Fig. 3: Microstructure of nickel super-alloy INCONEL 792-5A from the area of grain boundary

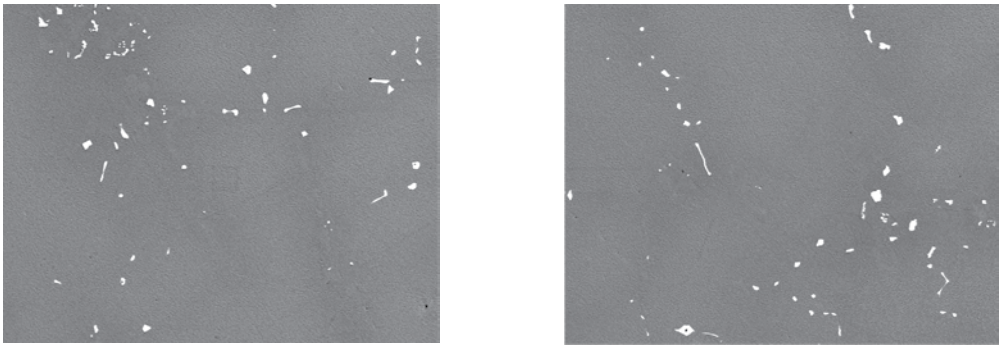

a) b)

Fig. 4: Primary carbides of the type MX in nickel super-alloy INCONEL 792-5A (reflected electrons)

Tab. 2 summarises data about chemical composition of the discussed carbidic particles, which confirm effect of increased contents of Ta and Ti. EDX spectrum of the observed particles is shown in the Fig. 5a.

Next Fig. 5.b shows and EDX spectrum, corresponding to coarser particles of the type $Ni_3$(Ti,Al) of γ' phase, which contribute to increase of physical-;metallurgical properties of nickel super-alloys.

Tab. 2: Chemical composition of primary carbides MX (at. %)

| Analysis No. | C | Ta | Mo | Ti |
|---|---|---|---|---|
| 1 | 48.9 | 25.5 | 1.9 | 23.7 |
| 2 | 47.7 | 23.5 | 1.3 | 27.5 |
| 3 | 45.5 | 26.0 | 1.3 | 27.3 |

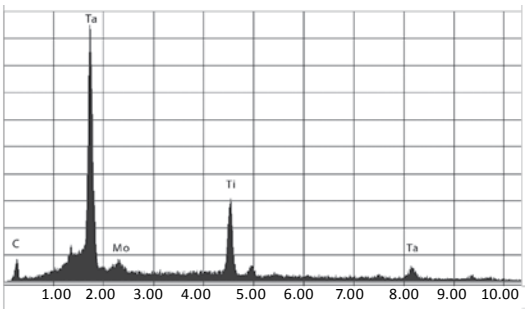


Fig. 5a: EDX spectrum of primary carbides MX – 792-5A

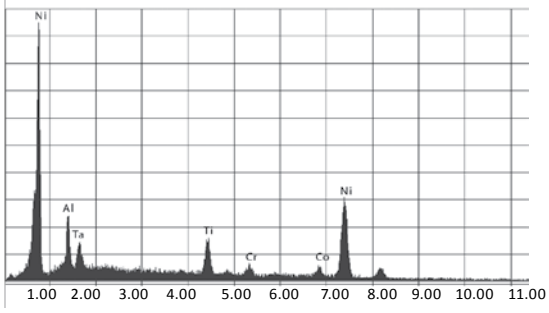


Fig. 5b: EDX spectrum of coarse particles Ni3 (Ti,Al) – 792-5A

Micro-structural anomalies formed by coarse particles in precipitate [3] were detected in inter-dendritic areas. Specific microscopically discerned elliptic formation follow from these areas and very fine particles of precipitate can be observed in them, as it is documented in Fig. 6a, b. Chemical analysis of the mentioned coarse particles in discussed areas leads to a conclusion that they are particles of the phase $Ni_3$ (Ti,Al ), as it is documented by the Tab. 3, or by record in the Fig. 5b. In the very vicinity of these micro-structural anomalies there were present areas with slightly reduced etchability, as it is documented e.g. by the Fig. 6b.

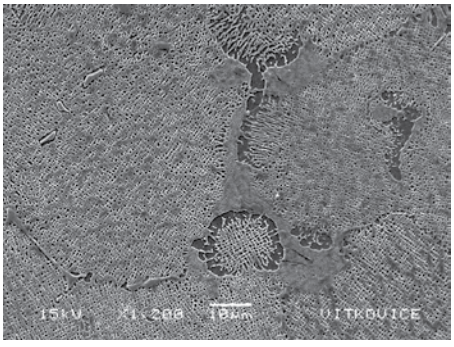


a)

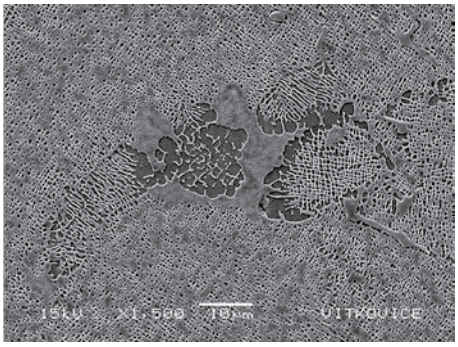


b)

Fig. 6: Microstructure of matrix – different etchability – INCONEL 792-5A

Tab. 3: Chemical composition of coarse particles (Al, Ti)Ni (at. %)

| Analysis No. | Al | Ta | Ti | Cr | Co | Ni |
|---|---|---|---|---|---|---|
| 1 | 12.2 | 3.4 | 9.0 | 3.4 | 6.9 | 65.1 |
| 2 | 12.1 | 3.2 | 8.7 | 3.5 | 6.4 | 66.1 |
| 3 | 11.5 | 3.1 | 9.2 | 3.9 | 6.6 | 65.7 |
| 4 | 11.6 | 3.1 | 9.1 | 3.4 | 6.4 | 66.4 |
| 5 | 11.6 | 3.3 | 8.2 | 3.7 | 6.6 | 66.6 |

Results of micro-chemical analysis of these areas and metallic matrix in the centre of crystallisation cells are given in the Tab. 4 and Tab. 5. It follows from the results that areas with partly reduced level of etchability are partly enriched by chromium, at average from approx. 16 at.% to 17.5-18 at.%, and on the other hand they are slightly depleted of the elements, which enrich the areas situated near the coarse particles of the phase γ'.

Particles of the precipitate $Ni_3$ (Ti, Al) were uniformly distributed in the basic metallic matrix of the given type of nickel super-alloy. Very fine particles were uniformly segregated also in the zones with reduced etchability, which occurred next to micro-structural anomalies having usually of elliptic form and containing coarse particles $Ni_3$ (Ti, Al).

Tab. 4: Chemical composition of metallic matrix (at. %)

| Analysis No. | Al | Ta | W | Mo | Ti | Cr | Co | Ni |
|---|---|---|---|---|---|---|---|---|
| 1 | 6.9 | 1.9 | 1.9 | 1.4 | 3.9 | 16.0 | 10.3 | 57.7 |
| 2 | 7.2 | 2.1 | 2.0 | 1.1 | 4.1 | 16.0 | 10.0 | 57.5 |
| 3 | 7.3 | 2.3 | 2.1 | 1.4 | 3.9 | 15.5 | 10.6 | 56.9 |

Tab. 5: Chemical composition in the areas with deteriorated etchability – in inter-dendritic zones in the vicinity of coarse particles (at. %)

| Analysis No. | Al | Ta | W | Mo | Ti | Cr | Co | Ni |
|---|---|---|---|---|---|---|---|---|
| 1 | 6.0 | 1.6 | 1.6 | 1.8 | 3.8 | 17.7 | 11.0 | 56.5 |
| 2 | 6.3 | 1.7 | 1.8 | 1.6 | 3.9 | 17.5 | 10.8 | 56.4 |
| 3 | 5.9 | 1.7 | 1.6 | 1.6 | 4.0 | 18.0 | 10.4 | 56.8 |

It can be stated that investigated super-alloy INCONEL 792 – 5A has comparable micro-structural characteristics as other types of nickel super-alloys. Its biggest contribution will probably consist in additional alloying of INCONEL 792 – 5A by tantalum and higher contents of cobalt. The first of these elements apparently contributes to formation of larger volumetric part of carbidic particles. Higher contents of cobalt can participate in increase of volumetric part of the phase γ' phase. Besides that its influence on reduction of stacking fault energy must not be ignored as it leads to enhancement of strength properties.

## CONCLUSION

In all it can be observed that although evaluated nickel super-alloy INCONEL 792 – 5A showed certain degree of micro-structural heterogeneity, in respect to the state of evaluated material and segregation characteristics of nickel super-alloys it is possible to assess the achieved level as good. Presented micro-structural analysis and evaluation of local chemical composition will contribute to more detailed knowledge of the given type of nickel super-alloy from the viewpoint of its technical applicability and possible following heat treatment.


## ACKNOWLEDGEMENT

The presented work was realised within the frame of the research plan MSM 6198910013 and project MPO FT-TA 3/072.


## Literature


Hrbáček, K.: Současný stav vývoje technologie přesného lití kol turbodmychadel ze superslitin na bázi niklu v naší republice [Current state of development of precision casting of discs for turbo-blowers from nickel super-alloys in our country], Research report, October 2005, 30 pp.

Hrbáček, K.: Výzkum a vývoj technologie přesného lití lopatek stacionárních plynových turbín, umožňující náhradu kovaných lopatek za lité [Research and development of technology of precision casting of blades of stationary gas turbines, enabling replacement of forged blades by cast blades]. Research report, Velká Bíteš, October 2005, 40 pp.

Jonšta, Z., Mazanec, K., Jonšta, P., Vodárek, V.: Strukturně fázová analýza niklových superslitin INCONEL 713LC a 792-5A, [Structural-phase analysis of nickel super-alloys INCONEL 713LC and 792-5A], Research report, VŠB-TU Ostrava, November 2006, 17 pp.

# A COMPARISON BETWEEN FINITE ELEMENT AND FINITE VOLUME METHODS ON THE STABILITY PROBLEM OF TIMOSHENKO BEAM

S. Isic, V. Dolecek, I. Karabegovic

## Abstract

This paper presents comparison of results of beam stability analysis obtained both by Finite Elements and Finite Volumes Method, where Timoshenko beam is considered. Methods are tested on the calculation of critical loads and corresponding buckling shapes. Results obtained by using these methods are compared on the basic of convergence speed, required mesh density, “shear locking” effect and calculation error.

## Key words

finite elements, finite volumes, stability, Timoshenko beam

Stability of beams is the standard problem in the stability analysis of elastic systems [1], but because of its importance, it is still a subject of research [2], [4]. Its importance arises from the fact that beams are part of many engineering structures for which design beam bending theory is needed. As the numerical method for its solution, in last few decades, Finite Element Method is commonly used [1], [2]. This method is well developed and gives good results for both Euler and Timoshenko beam. As one of disadvantages is “shear locking” effect in case of thin cross-sections of beams [2]. Finite Volume Method is more used in Computational Fluid Mechanics, and less attention is given to application of this method in solid mechanics, specially in stability analysis. Some works on its usage in analysis of beam bending and stability shows good results of this method in this area [4].

This paper presents a comparison of stability analysis of perfect Timoshenko beam, with uniform cross section loaded by axial force at one end, obtained both by Finite Elements and Finite Volume Method. Both methods use displacement based elements or volumes. Basic elements of deriving equilibrium equation for both methods are presented, and more attention is given to presentation of results and comparison of the methods. Methods are compared on the problem of calculation of critical loads and

buckling shapes for different characteristics of beams. Results obtained by using these methods are compared on the basis of convergence speed, required mesh density, "shear locking" effect, calculation error for pinned and clamped supports and different characteristics of beam cross section.

## FINITE ELEMENT ANALYSIS

- **Distretization of the domain into finite elements**

In case of finite elements analysis of considered problem, domain is divided into n beam finite elements with uniform cross-section with bending stiffness B, shear stiffness kAG and with two nodes at its ends. Nodes have two degrees of freedom, vertical displacement and rotation, which for i-th element are stored in element displacement vector

$$\{d\}^{ei} = \{w_i \; \theta_i \; w_{i+1} \; \theta_i{+}1\}^T.$$

Rotation of cross section is not equal to the derivative of vertical displacement, then, according to Timosenko beam bending theory, it differs for the shearing angle γ, i.e.

$$\theta = \frac{dw}{dx} - \gamma \,. \tag{1}$$

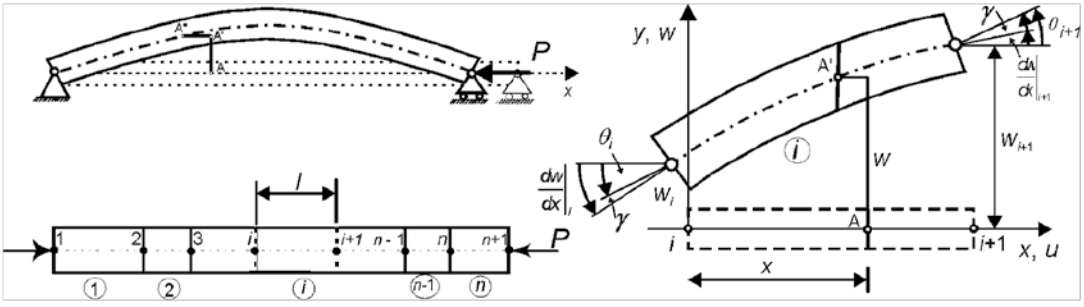


Fig. 1: Discretization of beam into finite elements with shearing effect.

Basic of finite elements method is shape matrix [N] [3], which is used to calculate displacements of arbitrary point inside the element from element displacement vector

$$\{u\} = [\mathbf{N}]\{\mathbf{d}\}^{e_i} \tag{2}$$

Shape matrix depends on chosen interpolation function. This paper uses both Bernouli and Mindlin finite element, because of their specific characteristics which are arising from interpolation function. Interpolation functions are given in Tab. 1.

Tab. 1: Interpolation functions for adapted Bernouli and Mindlin beam finite element.

| Bernouli element | Mindlin element |
|---|---|
| $w(x) = a_0 + a_1 x + a_2 x^2 + a_3 x^3$ | $w(x) = a_0 + a_1 x;\ \theta(x) = b_0 + b_1 x$ |

Interpolation function for Bernouli element is standard third-order polynomial function with four unknown constants as in case of Bernouli-Euler beams. To adapt this element for shearing effect, it must be used that that $a_3 = w'''(x)/6 = kAGy/(6B) = 2y/\phi/^2$.

In case of Mindlin finite element, interpolations of displacement and rotations are done separately by first order polynomial interpolation functions, and unknown constants are obtained directly from nodal displacement. Shear is included by using equation (1).

■ **Equilibrium equation**

When shape matrix is obtained, applying standard techniques in finite elements method, equilibrium equation could be derived in the form

$$\sum_{i=1}^{n}[\mathbf{k}]^{e_i}\{\mathbf{d}\}^{e_i} - P\sum_{i=1}^{n}[\mathbf{k}_\sigma]^{e_i}\{\mathbf{d}\}^{e_i} = 0\,, \quad (3)$$

where, element stiffness matrix $[k]^{ei}$ and geometry stiffness matrix $[k_\sigma]^{ei}$ for adapted Bernouli and Mindlin finite element are given in Tab. 2.

Tab. 2.: Stiffness and stress stiffness matrix for Bernouli and Mindlin finite element.

| | Bernouli element | | Mindlin element | |
|---|---|---|---|---|
| Coeff. | $\frac{EI}{l^3(1+\Phi)}[\mathbf{k}]^{e_i}$ | $\frac{1}{60l(1+\Phi)^2}[\mathbf{k}_\sigma]^{e_i}$ ] | $3kAG[\mathbf{k}]^{e_i}$ | $\frac{1}{2l}[\mathbf{k}_\sigma]^{e_i}$ ] |
| $(\,)_{11}$ | 12 | $2(36+60\Phi+30\Phi^2)$ | $12l$ | 1 |
| $(\,)_{12}$ | $6l$ | $6l$ | $6l^2$ | 0 |
| $(\,)_{13}$ | $-12$ | $2(-36-60\Phi-30\Phi^2)$ | $-12l$ | -1 |
| $(\,)_{14}$ | $6l$ | $6l$ | $6l^2$ | 0 |
| $(\,)_{22}$ | $(4+\Phi)l^2$ | $(8+10\Phi+5\Phi^2)l^2$ | $6B+2kAGl^2$ | 0 |
| $(\,)_{23}$ | $-6l$ | $-6l$ | $-3kAGl$ | 0 |
| $(\,)_{24}$ | $(2-\Phi)l^2$ | $-(2+10\Phi+5\Phi^2)l^2$ | $-6B+kAGl^2$ | 0 |
| $(\,)_{33}$ | 12 | $2(36+60\Phi+30\Phi^2)$ | $12l$ | 1 |
| $(\,)_{34}$ | $-6l$ | $-6l$ | $-6l^2$ | 0 |
| $(\,)_{44}$ | $(4+\Phi)l^2$ | $(8+10\Phi+5\Phi^2)l^2$ | $6B+2kAGL$ | 0 |

## FINITE VOLUMES ANALYSIS

■ **Distretization of the domain into finite volumes**

In case of FVM analysis of considered stability problem, domain is divided in n volumes with uniform cross-section, control point in the middle of volumes and additional two points at the ends of the domain. Point has two degrees of freedom, as it was case with nodal point of finite elements. Vector of displacement related to i-th volume is $\{d\}^{vi} = \{w_{i-1}\ \theta_{i-1}\ w_i\ \theta_i\ w_{i+1}\ \theta_{i+1}\}T$.

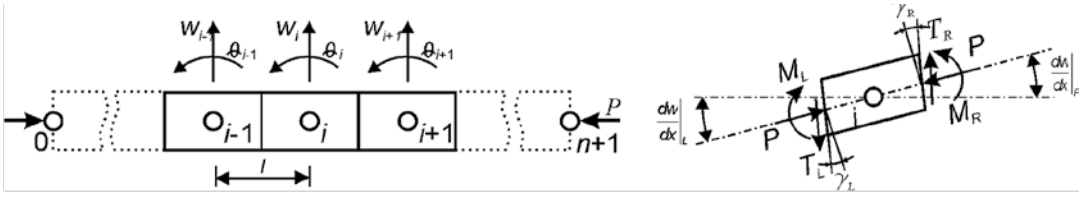


Fig. 2: Discretization of beam into finite volumes, and forces and moments acting on the volume.

■ **Equilibrium equation**

Equilibrium of transversal forces and moments on i-th finite volume may be written

$$-M_L + T_L \frac{l}{2} + T_R \frac{l}{2} + M_R = 0\,, \tag{4}$$

$$-T_L - P\frac{w_i - w_{i-1}}{l} + T_R + P\frac{w_{i+1} - w_i}{l} = 0\,, \tag{5}$$

Calculating forces and moments using central difference method as

$$M_L = B\frac{\theta_i - \theta_{i-1}}{l}; T_L = kAG\left[\left(\frac{w_i - w_{i-1}}{l}\right) - \left(\frac{\theta_{i+1} + \theta_{i-1}}{2}\right)\right] \tag{6}$$

$$M_R = B\frac{\theta_{i+1} - \theta_i}{l}; T_L = kAG\left[\left(\frac{w_{i+1} - w_i}{l}\right) - \left(\frac{\theta_{i+1} + \theta_{i-1}}{2}\right)\right] \tag{7}$$

equilibrium equation for the i-th volume may be written in the following matrix form

$$[\mathbf{k}]^{v_i}\{\mathbf{d}\}^{v_i} - P[\mathbf{k}_\sigma]^{v_i}\{\mathbf{d}\}^{v_i} = 0\,, \tag{8}$$

where, volume stiffness matrix [k]vi and geometry stiffness matrix $[k_\sigma]^{vi}$ are

$$[\mathbf{k}]^{v_i} = \frac{kGA}{l}\begin{bmatrix} 1 & -\frac{l}{2} & -2 & 0 & 1 & \frac{l}{2} \\ \frac{l}{2} & \frac{B}{kGA} - \frac{l^2}{4} & 0 & -2\frac{B}{kGA} - \frac{l^2}{2} & -\frac{l}{2} & \frac{B}{kGA} - \frac{l^2}{4} \end{bmatrix},$$

$$,[\mathbf{k}_\sigma]^{v_i} = \frac{1}{l}\begin{bmatrix} 1 & 0 & -2 & 0 & 1 & 0 \\ 0 & 0 & 0 & 0 & 0 & 0 \end{bmatrix}.$$

Writing equation (8) for all volumes give equilibrium equation of the beam. Matrices are slightly different for volumes at the end of the domain, where distance between points is *l*/2 and boundary conditions are introduced.

## COMPARISON OF METHODS

Equilibrium equations (3) and (8) derived by using both methods have the form of algebraic eigenvalue problem of equal sizes for same number of elements and volumes. Equilibrium equations for unknown lowest critical force and buckling shape are solved using Power method vv[5], for what computer code is written. Presented examples use elements and volumes of equal length. Examples of comparison are done for beams with pinned and clamped supports and cross section and cross-sections with significant influence of shear.

■ **Example 1: Simple beam**

Results of calculation of critical force and corresponding buckling shape for simple beam is presented in Fig. 3 and Fig. 4. Fig. 3 shows fast convergence of finite element method based on adapted Bernouli element (FEM1), and very slow convergence in case of Mindlin element (FEM2). Finite volume method also converges fast, with greater number of volumes than in finite elements method FEM1. The same results for buckling shape by using these methods are calculated (Fig. 4), where FEM calculates displacement at the ends of elements and FVM in the middle of volumes.

Results of calculation of critical load for simple beam for different height of cross section are presented in the Fig. 5. Number of elements are increased to achieve precision of calculation of critical force with relative error less than 1%. Finite element analysis based on Bernouli element and finite volume method show insensitivity on beam slenderness. Increasing of height of cross section causes slow increasing of necessary number of elements, while in case of finite volume, desired accuracy is possible to obtain with the same number of volumes. Mindlin finite elements is appropriate only for thick beams, while for thin beams the required number of finite elements is very large and makes this element almost unusable in this case.

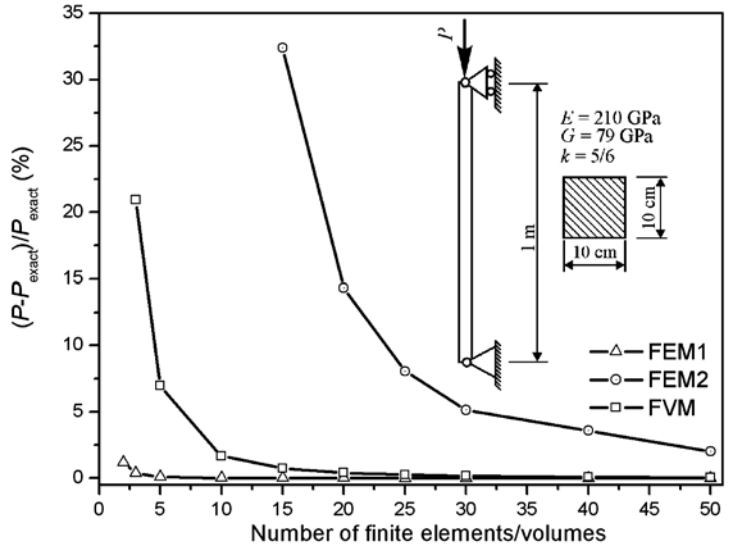


Fig. 3: Necessary mesh density for convergention of critical force to exact value.

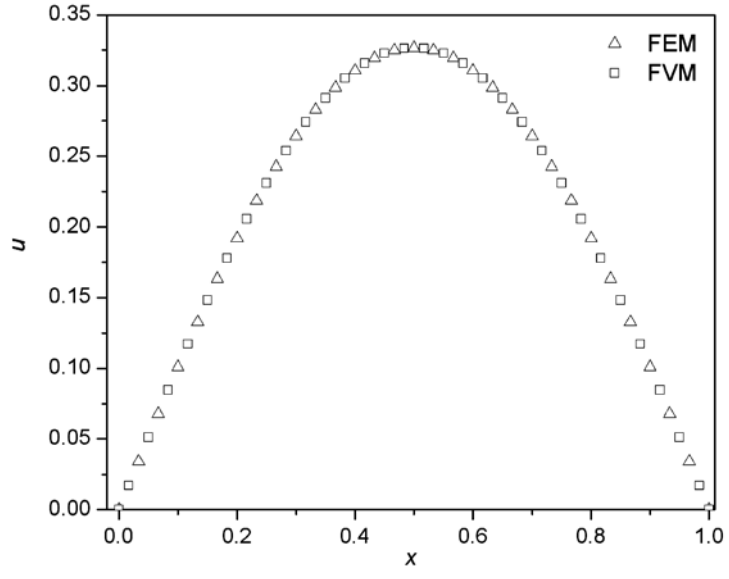


Fig. 4: Buckling shape of simple beam calculated by finite elements and finite volume method.

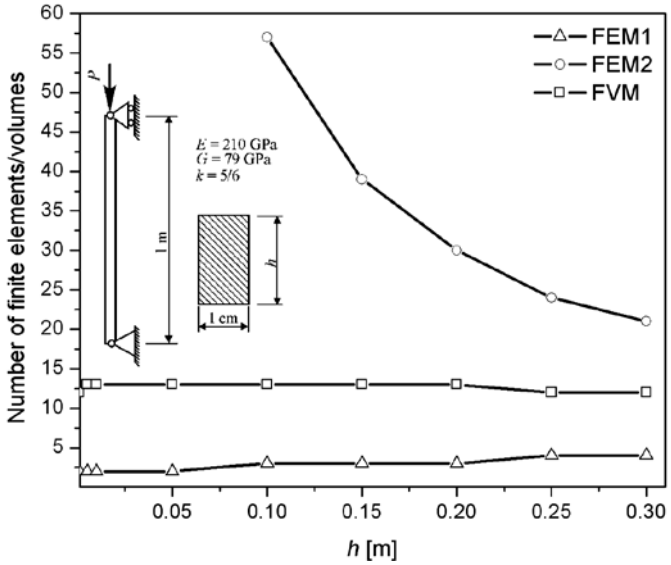


Fig. 5: Neccesary mesh density for calculation of critical force with relative error less then 1%.

■ **Example 2. Clamped-Pinned beam**

Another problem for testing methods is clamped-pinned beam. Results of calculation of critical force and buckling shape are shown on Fig. 6 and Fig. 7 for beam with given characteristics. Critical force is compared to exact Euler value.

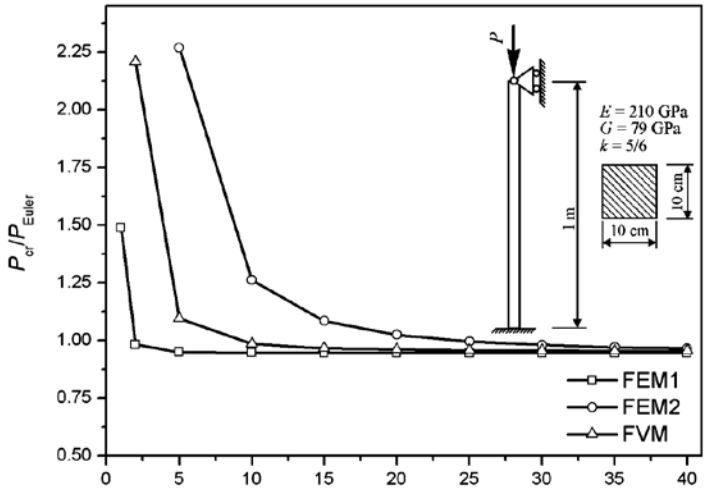


Fig. 6: Necessary mesh density for convergention of critical force to the exact value.

Results shows similar convergence rate as in the previous example, i.e. fast convergence of FEM1 and FVM, and slow convergence of FVM2. Calculated buckling shape for beam considered in this example is equal in case of both method (Fig. 7).

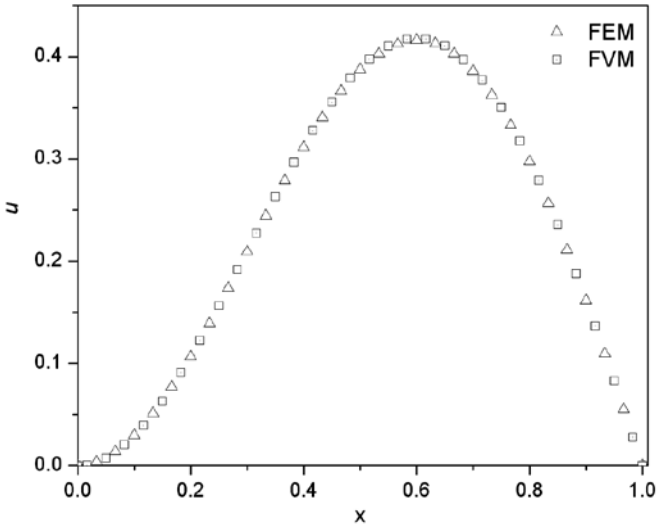

Fig. 7: Buckling shape of pinned-clamped beam calculated by finite elements and finite volume method.

## CONCLUSIONS

This paper presented comparison of method of finite elements and finite volumes on the stability analysis of Timosenko beam. In case of finite element analysis two kinds of finite elements – Bernouli and Mindlin beam finite element are considered. For both methods short outlines for derivation of equilibrium equation are presented. Critical force and corresponding eigenvector is calculated using Power method.

Comparison shows that convergence of results is the fastest case of finite elements analysis based on adapted Bernouli finite element, which is insensitive to "shear locking effect". Fast convergence lies in the fact that interpolation function allows parabolic change of the bending moment along element. One disadvantage is that adaptation for shearing may be done only if constant shearing angle over element is considered.

Mindlin finite elements leads to simpler constitutive matrices, but exploit very slow convergence and high sensitivity to shear locking effects in case of thin beams.

Finite volume method converges slower than finite element method with Bernouli element, but it is insensitive to shear locking effect and constitutive matrices in equilibrium equation are simpler and sparser than in the case of finite elements. Method allows both linear change of bending moment and shearing force over volumes.

J.M.T. Thompson, G.W. Hunt, “A General Theory of Elastic Stability”, John Wiley & Sons, 1973.
Cook R., Malkus D.S., Plesha M, ‘’Concepts and Application of Finite Element Analyses’’, John Willey & Sons, New York, 1988.
S. Isic, V. Dolecek, I. Karabegovic, “Numerical And Experimental Analysis Of Postbuckling Behaviour Of Prismatic Beam Under Displacement Dependent Loading”, Proceedings of the First Serbian Congress on Theoretical and Applied Mechanics, Kopaonik, Serbia, 2007.
N. Fallah, F. Hatami, “Extension of the Finite Volume Method for Instability Analysis of Columns with Shear Effects”, Proceedings of the Eighth International Conference on Computational Structures Technology, Civil-Comp Press, Stirlingshire, Scotland, 2006.
A. Jennings, J.J. McKeown, Matrix Computation, John Willey & Sons, 1992.

# ION EXCHANGED, HIGH-STRENGTH GLASS COMPONENTS

D. Hülsenberg, Y. Ludwig, S. Mrotzek

## Abstract

The tests were made with a photostructurable glass containing $Li^+$-, $Na^+$- and $K^+$-ions. The last step to make the microstructured glass components is an acid treatment which already enables them to a higher strength compared with window glass. For further increase of strength the ion exchange in melted, different nitrates was used. If in the layers near to the surface ions of a smaller radius are exchanged against such of a greater one, compressive stresses are generated in the ion exchanged layers. They compensate tensile stress during the application and can enlarge the bending strength of the glass components up to nearly 800 M Pa.

## Key words

strength, ion exchange, microstructured glass, diffusion, fine annealing

It is very well known that glass products are brittle and exhibit a low, scattering strength. The reason of this behaviour is the anion-cation-structure of anorganic-nonmetallic glasses which excludes a plastic deformation if stressed. Because any real glass product has micro cracks and flaws in its inner and near the surface an externally applicated tensile stress opens the cracks and creates stress maxima in its origin, see Fig. 1. Of course these maxima may be much greater compared with the measured average stress. They are the reason for glass breaking much earlier as expected. The real stress $\sigma_r$ depends on the applicated average tensile stress $\sigma_z$, the half crack length a and the crack radius r in its origin, as given in Eq. (1):

$$\sigma_r = 2\,\sigma_z \sqrt{\frac{a}{r}} \qquad (1)$$

As larger r and as smaller a as smaller becomes $\sigma_r$. This fact is very well known and used in etching glass products to eliminate the surface cracks. An other possibility to improve the strength of glass products (not of the glass material itself) is the application of implemented in the surface layer compressive stress in order to close the cracks

at least so long until the tensile stress exceeds the implemented compressive stress in the surface. This compressive pre-stress can be generated by thermal hardening or by ion exchange [1, 7, 8]. The produced stress profiles are drawn in Fig. 2.

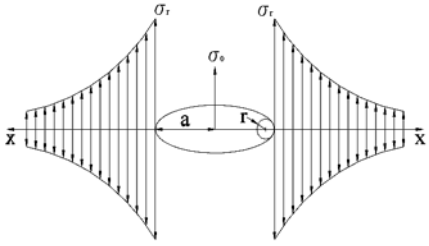


Fig. 1: Stress in dependence on the distance from the crack ends

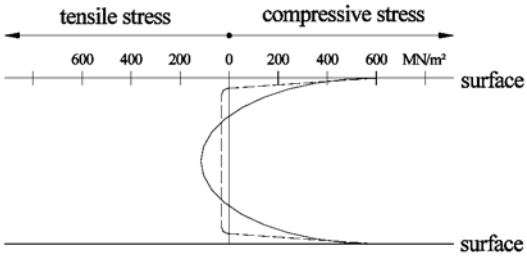


Fig. 2: Stress profiles in a glass component after a thermal hardening (continuous line) or ion exchange (dotted line) [8]

## GLASSPROBES

There are many progressions in the microstructuring of glasses [3, 4, 6]. But the application of the components frequently fails because of prejudices concerning the mechanical properties. Although it is very well known that glass fibers exhibit a much higher strength compared with specimens (DIN 52303) made from window glass, the applicator is not prepared to suppose this fact also for microstructured glass components. Therefore we have measured the strength of as received microstructured glass components and after an ion exchange without and with fine annealing the components during microstructuring. The method to do so was a modified photolithography of a masked UV-sensitive glass. Its composition is given in Tab. 1.

Tab. 1: Composition of the used UV-sensitive glass

| main components | | dopands | |
|---|---|---|---|
| oxide | mass-% | oxide | mass-% |
| $SiO_2$ | 74.29 | $Sb_2O_3$ | 0.40 |
| $Al_2O_3$ | 7.20 | $Ag_2O$ | 0.12 |
| $Li_2O$ | 11.61 | SnO | 0.07 |
| $Na_2O$ | 2.74 | $CeO_2$ | 0.03 |
| $K_2O$ | 4.16 | | |

The principle of microstructuring is the following: The melting regime enables to generate $Ce^{3+}$ and $Ag^+$. The glass melt is pressed to form disks which are ground and polished. They are covered with a removable quartz glass mask. If applicating UV-radiation of the wavelength between 300 and 320 nm, in the exposed regions (holes in the mask) $Ce^{3+}$ delivers a photoelectron to $Ag^+$, which becomes atomic silver. The silver atoms exist only in the exposured places. They are much more movable in the glass compared with silver ions. If heating the glass disk, e. g. up to 500 °C, the silver

atoms diffuse and generate silver clusters. Possessing a diameter of nearly 7 nm, these clusters if being located in so called phase separation droplets act as crystal nuclei for $Li_2O$ . $SiO_2$-crystals. During a following thermal treatment, e. g. at 570 °C, these crystals are growing. Their diameters between 100 nm and 1 µm depend on the chosen conditions of the thermal treatment, see [6]. Because of the very easy solubility of the $Li_2O$ $SiO_2$-crystals in hydrofluoric acid it is now possible, to etch off the crystals and – in doing so – to microstructure the glass in the UV-exposured regions. Fig. 3 shows a microstructured glass component and Fig. 4 an array of 12 specimens for tests.

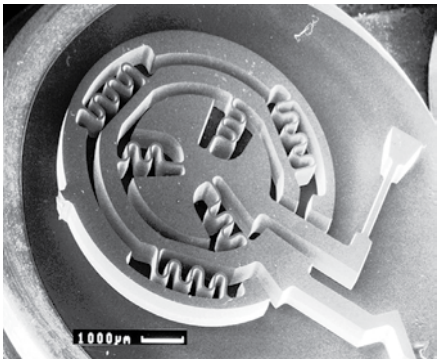

Fig. 3: Middle ear implant made from UV-stucturable glass

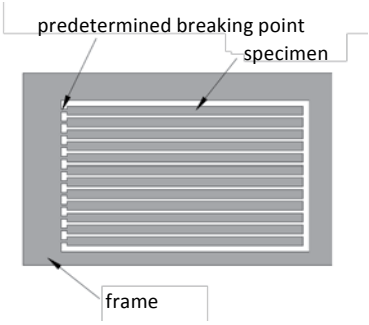

Fig. 4: Array of 12 specimens for bending test

These 12 specimens are broken out of the frame for bending tests in the as received state, or the complete frame including specimens is subjected to the ion exchange.

## PROCEDURE OF ION EXCHANGE

The aim was to realize the ion exchange at temperatures below the strain-point (383°C, [2]) of the glass in order to prevent a compressive stress annealing in the surface near layers by flowing during the ion exchange. The lowest reaction temperature is given by the melting point of the used salts ($LiNO_3$, $NaNO_3$ and $KNO_3$). As expected, the ion exchange in $KNO_3$ melts generates the highest compressive pre-stress. Therefore only these results will be reported. The reason for this effect is the great ion radius of $K^+$ ($r_{Li}+ = 78$ pm, $r_{Na}+ = 98$ pm, $r_K+ = 133$ pm). If replacing $Li^+$ or $Na^+$ by $K^+$, the later ion needs much more volume in the glass network compared with the other both, what generates compressive stress in the exchanged layers. It is necessary to find an optimum of temperature which is high enough for $K^+$-diffusion and low enough to avoid flowing. The procedure took place in a corrosion stable steel crucible positioned in a laboratory furnace. The micro structured glass specimen array was dipped into the melt and treated at temperatures between 345 up to 420 °C for ½ up to 48 hours. After each procedure the salt melt (300 g) was renewed. Two arrays of specimen were hanged up on a platinum frame in each exchange test. Following 24 specimen could be tested and used to calculate an average value of the bending strength at each testing point and of its scattering.

Specimen of a cross-section of nearly 1 x 1 $mm^2$ and a support distance of 2 cm were used for three-point-bending tests.

## RESULTS

Because of the small dimensions of the specimen compared with the requirement of the DIN 52303 and because during making the specimen by photo structuring (the last step is as mentioned above an etching in hydrofluoric acid what avoids the generation of surface cracks and flaws) already the as received specimen have a bending strength of 340 ± 30 MPa. This is very high compared with commercially available glass tested by DIN (60 … 80 MPa). That means, that – without post-treatment – microstructured glass components have a respectable strength.

The results after ion exchange for 30 min at different temperatures are given in Fig. 5.

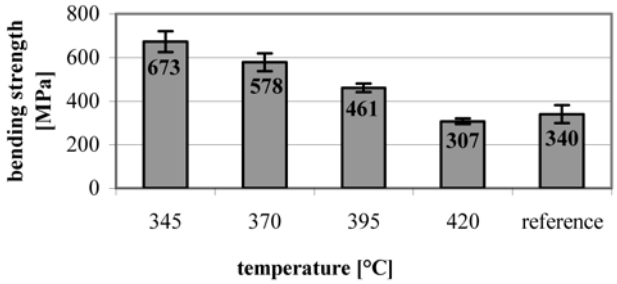


Fig. 5: Bending strength of specimen after an ion exchange in KNO3-melts for 30 min at different temperatures

The strength is in maximum doubled compared with the untreated specimen. The effect diminishes with increasing temperature of ion exchange. A temperature of 345 °C is high enough for ion exchange by diffusion. The in-diffusing $K^+$-ions generate a compressive stress which compensates at the beginning of the bending test the tensile stress at the under site of the bar. This fact is the reason for the very high measured bending strength. If the exchange temperature is enhanced, the diffusion is more activated, but at the same time the glass starts to flow (annealing point = 383 °C). The as created stress anneales more and more. An elongation of the residence in the salt melt from ½ to 48 hours has a similar effect.

The evidence of the ion exchange as reason for the enhanced bending strength is given in Fig. 6.

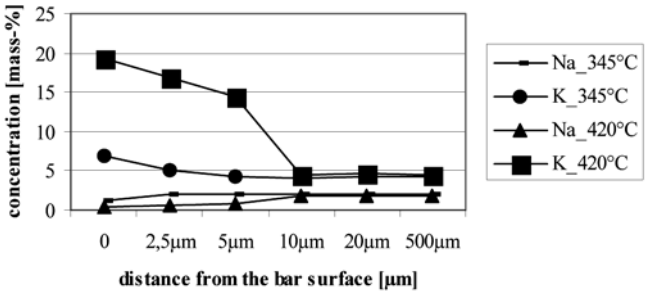


Fig. 6: $K^2O$- and $Na^2O$-concentrations in dependence on the distance from the specimen surface (0 = surface) after 30 min treatment in melted $KNO_3$

It is clearly visible that the $K_2O$-concentration at the surface of the glass specimens increases and the $Na_2O$-concentration decreases. The difference in concentration is caused by the not measurable $Li_2O$-profile. At 345 °C the diffusion depth is 5 µm, at 420°C 10 µm. But all effects at 420 °C are annealed by flowing. Therefore the best ion exchange conditions in $KNO_{3-}$melts are 345°C for 30 min.

Additional tests were made by varying the microstructuring procedure. Between the thermal treatment for crystal growing and the etching we have inserted a so called fine cooling or annealing. It is a process commonly used for making stress free and more homogeneous, optical glass products. In our case we have expected more phase separation droplets and an influence on the silver-nucleation. The fine cooling (annealing) consists of the steps: Heating up to 480°C with 8 K/min, 30 min residence time and again cooling to room temperature with 2 K/min. After the etching the ion exchange took place as described. The bending strength was very surprising, 777 ± 70 MPa, that means, once more an enhancement. The results in more details are given in [5].

## SUMMARY

Microstructured glass components have originally a higher strength compared with common glass products. The reasons are the geometry of the test probes and the prevention of surface flaws by etching. An ion exchange in surface near layers, if ions with a greater radius replace such ones with smaller radius and, in doing so, create a compressive pre-stressed layer, causes an increase of bending strength to 673 ± 47 MPa. The best conditions for the ion exchange are 30 min at 345 °C in a $KNO_3$ melt. If a fine cooling (annealing) is inserted between the growth of $Li_2O$ . $SiO_2$-crystals and their etching off, the strength of the test specimens once more increases to 777 ± 70 MPa.

## Literature

Burggraf, A. J.: The mechanical strength of alkali-alumosilicate glasses after ion exchange. Philips Res. Rep. Suppl. 1966, No. 3, pp. 1 - 106

Hecht-Mijic, S.: Brechzahländerung durch Ionenaustausch in strukturierten Glasbauteilen. Doctor-thesis, TU Ilmenau, 2003

Hesse, A.: Modifizierung von fotostrukturierbarem Glas durch partielle Kristallisation. Diploma-thesis, TU Ilmenau, 2004

Ludwig, Y.: Parameteruntersuchungen zum Ätzprozess von fotostrukturierbarem Glas. Project-thesis, TU Ilmenau, 2003

Ludwig, Y.: Modifizierung von fotostrukturiertem Glas durch Ionenaustausch. Diploma-thesis, TU Ilmenau, 2004

Mrotzek, S.: Kristallisation eines UV-strukturierbaren Glases im System Li2O-Al2O3-SiO2. Doctor-thesis, TU Ilmenau, 2005

Scholze, H.: Glas – Natur. Struktur und Eigenschaften. Springer Verlag, Berlin, 1977

Spauszus, S.: Werkstoffkunde Glas. VEB Deutscher Verlag für Grundstoffindustrie, Leipzig, 1974

# PHOTOLUMINESCENCE AND RAMAN SPECTRA OF $70TEO_2•30PBCL_2$ GLASSES DOPED WITH $PR^{3+}$

I. Furár, V. Trnovcová, M. Kadlečíková, J. Pedlíková

## Abstract

Tellurite glasses, $70TeO_2.30PbCl_2$ (7T3P), were prepared in Au and Pt crucibles. $Pr^{3+}$ ions were added in different chemical forms (metals, chlorides, oxides), in concentrations of 500 – 1500 wt-ppm. In the range of 640-700 nm, six photoluminescence (PL) peaks were observed, at 641.5, 647.1, 652.4, 660.8, 662.9, and 664,5 nm, both in pure and doped glasses. In the wave number range of 200 – 1200 $cm^{-1}$, seven Raman scattering (RS) peaks were observed, at 184, 217, 321, 468, 654, 735 $cm^{-1}$, and a small peak at 650 $cm^{-1}$. Both spectra were deconvoluted using symmetrical Gaussian functions. Energies, amplitudes and half-widths of band maximums were free parameters. Doping with $Pr^{3+}$ or reactions with crucibles result in structural changes of tellurite polyhedrons. The influence of $Pr^{3+}$ on the local structure is similar to that of incorporated $Au^{+}$. Relative intensities of PL bands and RS ones depend on the concentration of $Pr^{3+}$ and on the material of the crucible. Positions of these bands are independent of $Pr^{3+}$ concentration and of the crucible.

## Key words

tellurite glasses, $Pr^{3+}$ doping, photoluminescence, Raman spectrum, Au, Pt crucibles

Tellurite glasses are of a great scientific and technological interest due to their promising physical properties [1]. Their most important advantages are: wide transmission range (≈400 nm to 15 μm), lack of toxicity, good glass stability and strength, corrosion and moisture resistance, low phonon energy (≈ 800 $cm^{-1}$), high density (≈ 5.5 $g/cm^3$), and high refractive index (≈2). The glasses can be used in optical components (windows, prisms, laser glasses) or in fiber optics communications. In binary and ternary systems, heavy ions influence the absorption ability of glasses. They shift the IR cut-off towards longer wavelengths. The aim of this work is to present the photoluminescence and Raman spectra of tellurite/lead chloride glasses, $70TeO_2·30PbCl_2$, doped with $Pr^{3+}$ ions, in various concentrations and chemical forms, prepared in Pt or Au crucibles. Experimental results are discussed from the point of view of the microstructure and optical properties of glasses.

## EXPERIMENTAL DETAILS

Studied tellurite/lead chloride glasses, $70TeO_2 \cdot 30PbCl_2$ (7T3P), were prepared using the method of a „divided ampoule“ [2]. They were doped with praseodymium (0 - 1500 wt-ppm), which was added as metal (Pr), chloride ($PrCl_3$) or oxide ($Pr_2O_3$). Glasses were prepared in Pt or Au crucibles. Samples prepared in Pt crucibles were orange; those prepared in Au crucibles were yellowish.

Photoluminescence (450-700 nm) and Raman (150-3000 $cm^{-1}$) scattering measurements were made using Raman spectrometer Dilor-Jobin Yvon-Spex, type LabRam. He-Ne laser (632.8 nm) was used as the excitation source at room temperature.

## RESULTS AND DISCUSSION

Influences of the crucible and $Pr^{3+}$ concentration (in a metallic form) on the PL spectrum of 7T3P glasses are shown in Fig. 1a or 1b, respectively. The influence of a chemical form of $Pr^{3+}$ on the photoluminescence (PL) spectra is shown in Fig. 2. Experimental dependences were fitted by a sum of Gaussian distributions. Energies of band maximums, amplitudes and half-widths were free parameters. In the range of 640-700 nm, six

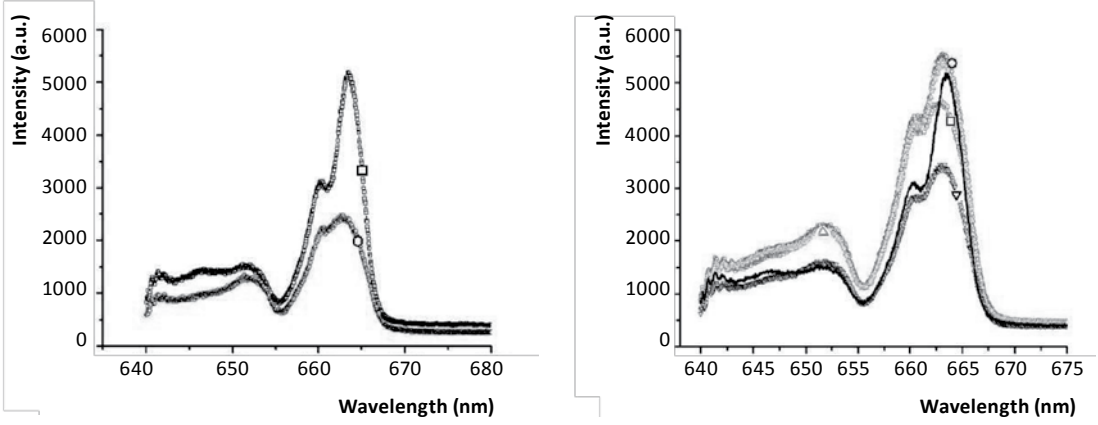


Fig. 1: Photoluminescence spectra of 7T3P glasses a)”pure” glasses, prepared in a Pt (□□□, black) or Au (ooo, red) crucible; b) glasses prepared in Pt crucibles, doped with Pr in a metallic form (□□□ (brown) 500 wt-ppm, ooo(red) 800 wt-ppm, ΔΔΔ (green) 1000 wt-ppm, ▽▽▽ (blue) 1500 wt-ppm, full line – “‘pure”)

PL peaks, centered at 641.5(1), 647.1(4), 652.4(1), 660.8(2), 662.7(4), 664.5(2) nm, were observed, both in pure and doped glasses. The same positions of these bands were found in glasses prepared in both gold and platinum crucibles. However, relative intensities of these bands depended on the chemical form and concentration of Pr3+, and on the material of the crucible. Origin of these bands is not clear. Short and long wavelength bands could be attributed to 3P0→3F2 or 3P1→3F3 transitions in $Pr^{3+}$ ions, respectively [3,4], provided that “pure” glasses contain traces of $Pr^{3+}$.

In Figs. 3, 4, Raman spectra of the T7P3 glasses are presented. No systematic influence of the crucible or $Pr^{3+}$ doping in any chemical form on the positions of RS bands was observed. Six Gaussian bands, centered

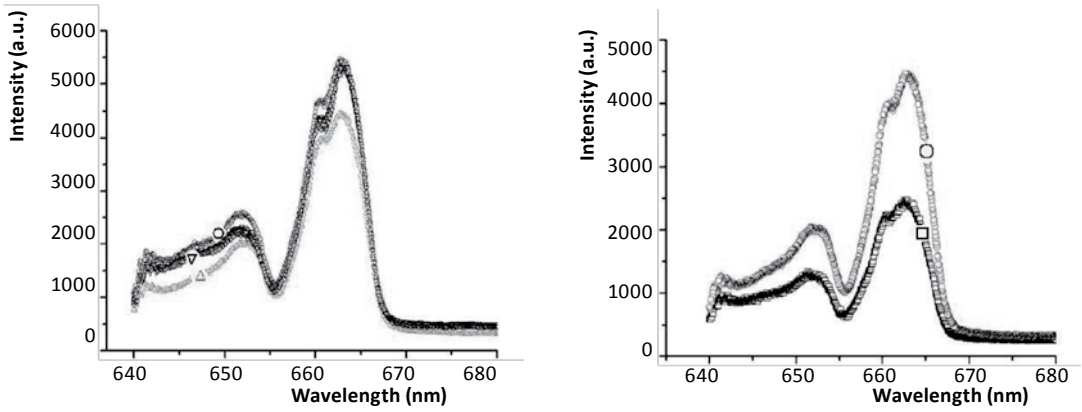


Fig. 2: Influence of the chemical form of Pr on the PL spectra of 7T3P glasses prepared in a/ Pt crucibles (▽▽▽ (blue) 1000 wt-ppm $Pr_2O_3$, ooo (red)1000 wt-ppm $PrCl_3$, ΔΔΔ (green) 1000 wt-ppm Pr), b/Au crucibles ( □ □ □ "pure" (black), o oo (red) 1000 wt-ppm PrCl3)

at 184(2), 217(7), 321(2), 468(2), 654(9), 735(5) $cm^{-1}$ and one small peak at 650 $cm^{-1}$ were determined (Fig. 5). (Only peaks of "pure" T7P3 glass prepared in a Pt crucible are slightly shifted to smaller wavenumbers). In the range of 350-900 $cm^{-1}$, the spectra are similar to those of $TeO_2$-based glasses [5-7], only intensities of dominant peaks at 735 and its shoulder at 654 $cm^{-1}$ are interchanged. The peaks at 735 and 654 $cm^{-1}$ are usually attributed to $TeO_3$ trigonal pyramids (tp) or $TeO_4$ trigonal bipyramids (tbp), respectively. The small peak at 650 $cm^{-1}$ probably comes from intermediate $TeO_{3+1}$ polyheders. These structural units are connected each other with their corners into linear or ring chains. The peak at 468 $cm^{-1}$ is attributed to symmetric stretching of Te-O-Te links [8]. $Pb^{2+}$ ions act as network modifiers. The peak at 322 $cm^{-1}$ can be probably assigned to Pb-Cl vibrations. Peaks at low frequencies are Bose peaks or spurious effects.

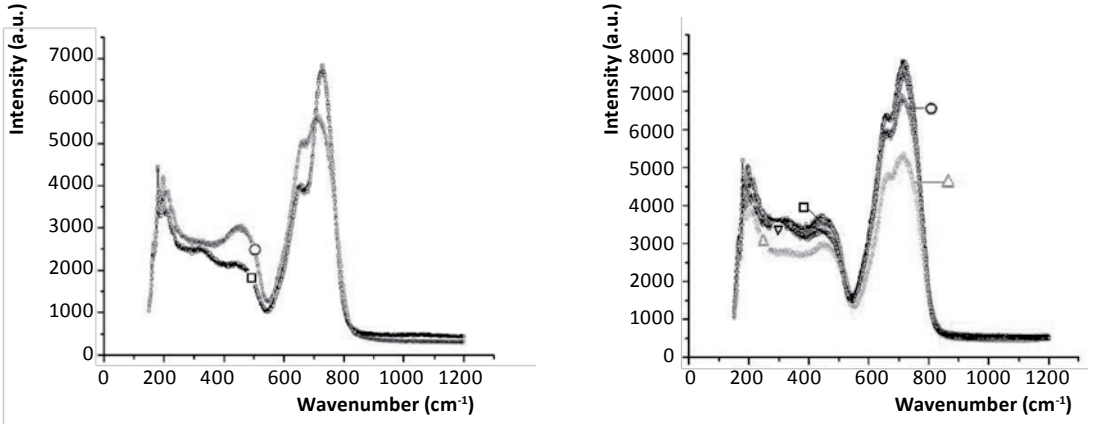


Fig. 3: Raman spectrum of 7T3P glasses, a) "pure" glasses, prepared in a Pt ( □ □ □ ) or Au (ooo) crucible, b) doped glasses with 1000 wt-ppm $Pr_2O_3$ ( □ □ □ ), 1000 wt-ppm $PrCl_3$ (ooo), 1000 wt-ppm Pr (▽▽▽), prepared in Pt crucibles, and 1000 wt-ppm $PrCl_3$ (ΔΔΔ), prepared in Au crucibles

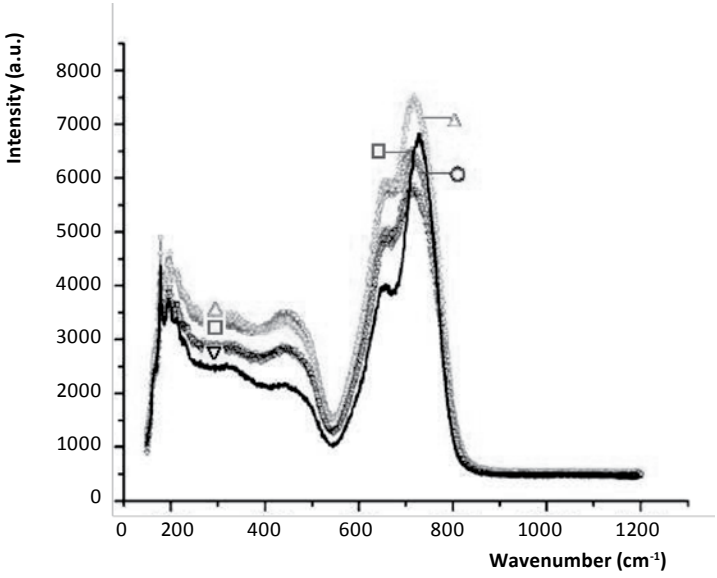


Fig. 4: Raman spectra of 7T3P glasses, prepared in Pt crucibles, doped with metallic Pr (□□□ 500 wt-ppm, ooo 800 wt-ppm, ΔΔΔ 1000 wt-ppm, ▽▽▽- 1500 wt-ppm, full line – "pure" glass)

Relative intensities of the peaks depend on doping and on the material of the crucible. In glasses prepared in gold crucibles, the peak at 468 $cm^{-1}$ is more pronounced than those in glasses prepared in Pt crucibles. Also the tbp (654 $cm^{-1}$) peak is more pronounced compared to tp (735 $cm^{-1}$) peak in glasses prepared in gold crucibles. Doping of glasses prepared in gold crucibles does not change substantially their Raman spectrum. Doping of glasses prepared in Pt crucibles increases intensities of both the peak at 468 $cm^{-1}$ and that one at 654 $cm^{-1}$. Spectra of doped glasses prepared in different crucibles are more similar than spectra of "pure" glasses. It seems that reactions with crucibles and a fast diffusion of Au result in serious structural changes in tellurite polyhedrons. The influence of $Pr^{3+}$ and $Au^{+}$ on the structure of glasses is similar.

## CONCLUSIONS

Reactions with crucibles result in serious changes in tellurite structural units. Influences of $Pr^{3+}$ and $Au^{+}$ on the glass structure are similar. In the range of 500-700 nm, six PL peaks were found both in "pure" and doped T7P3 glasses. In the range of 200 – 1200 $cm^{-1}$, seven RS bands were detected. Relative intensities of both PL and RS peaks depend on the concentration of Pr and on the material of the crucible. They indicate ratios of concentrations of various structural units in glasses. Three RS peaks are assigned to vibrations of $TeO_4$ polyhedrons. One RS peak is attributed to symmetric stretching of Te-O-Te links The peak at 322 $cm^{-1}$ can be probably assigned to Pb-Cl vibrations.

## ACKNOWLEDGEMENT

The work was supported by the Scientific Grant Agency VEGA, Slovak Republic, project no. 1/2000/05.

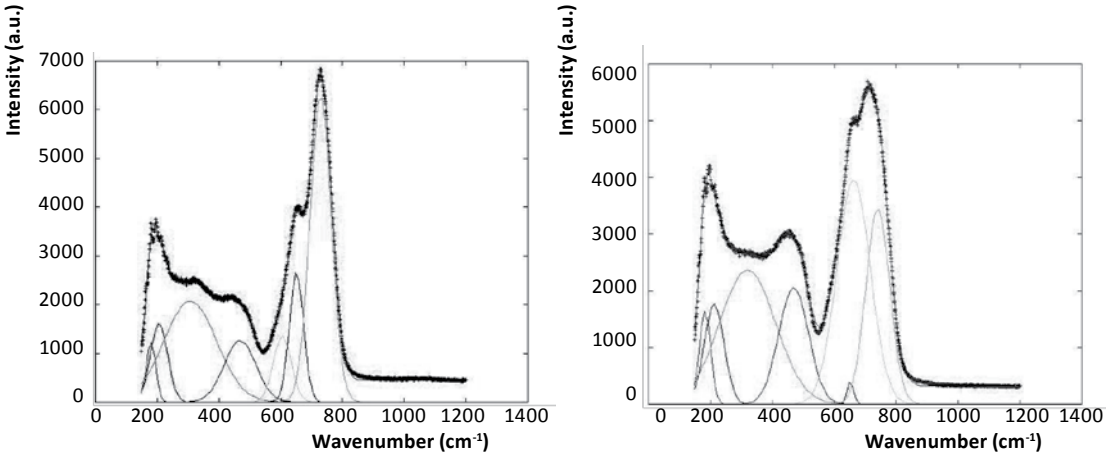


Fig. 5: Deconvolution of Raman spectra in undoped tellurite glasses (70 $TeO_2$•30$PbCl_2$) prepared in a/ Pt, b/ Au crucibles.

## Literature


O'Donnell, M. D., Miller, C. A., Furniss, D., Tikhomirov, V. K. & Seddon, A. B.: Fluoro telluride glasses with improved mid-infrared transmission. J. Non-Cryst. Solids, 331, 2003, 48-57

Pedlíková, J., Ležal, D., Kostka, P. & Zavadil, J.: Glasses based on TeO2 and $Pb^{2+}$: preparation and characterization. J. Non-Cryst. Solids, 326, 2003, 42-46

Ravi Kumar, V., Veeraiah, N., Appa Rao, B.: Optical absorption and photoluminescence properties of $Pr^{3+}$ doped $ZnF_2$-PbO-$TeO_2$ glasses. J. Lumin., 75, 1997, 57-62

Moorthy, L.R., Jayasimhadri, M., Radhapathy, A., Ravikumar, R.V.S.S.N.: Lasing properties of $Pr^{3+}$ doped tellurofluorophosphate glasses. Mater. Chem. Phys., 93, 2005, 455-460

Marjanovic, S., Toulouse, J., Jain, H., Sandmann, C., Dierolf, V., Kortan, A.R., Kopylov, N., Ahrens, R.G.: Characterization of new erbium doped tellurite glasses and fibers. J. Non-Cryst.Solids. 322, 2003, 311

Jeansannetas, B., Blanchandin, S., Thomas, P. & et al.: Glass structure and optical nonlinearities in Thallium (I) Tellurium (IV) oxide glasses. J. Solid State Chem. 16, 1999, 329-335

Lin, J., Huang, V., Sun, Z.G., Ray, CH.S., Day, D.E.: Structure and non-linear optical performance of TeO2-Nb2O5-ZnO glasses. J. Non-Cryst. Solids, 336, 2004, 189-194

# PREPARATION OF SANDWICH MATERIALS MADE BY EXPLOSIVE CLADDING

L. Čížek, M. Tvrdý, S. Król, S. Szulc, R. Bański, A. Hernas

## Abstract

Paper presents results of investigations with three-layer explosively formed sandwich composite called trimetal consisting of steel, titanium and aluminium. Obtained joint represents high mechanical properties and good workability. Production of so-called welding connectors is one of possible areas of explosive welding application. Generally, the welding connectors are metal composites having e.g. steel layer from one side and aluminium or aluminium alloy layer from the other. Structure and properties after explosive welding have been analysed as influence of annealing on conversions in and properties of bonding zones and bonded materials. It has been proved that elaborated parameters of explosive system ensure complete welding both in steel-titanium and titanium-aluminium regions. The microstructure changes of this Sandwich Steel-Ti-Al area have been investigated using light microscopy.

## Key words

sandwich metals, explosively formed composite, structure, properties

Protective of metal surface has significant role in application of materials in corrosion medium. Usual used stainless steels in the case of heavy products are very expensive. From this reason often is sufficient create thin layer from this material on the surface of usual material. One of methods applied for creating such sandwich materials is explosive welding application [1-3]. Way of explosive join is made in cold state. Application of explosive welding enables bonding of different, mutually unweldable metals [4-6]. Obtained joint represents high mechanical properties and good workability. Plastic materials have very good assumption for explosive joining and joint has very good mechanical properties. The thickness of joint can reach from some tenth to thirty mm.

From the reason arising of joint below melting point of metals we can join very different metals materials.

Principle of explosive cladding is shown in Fig. 1.

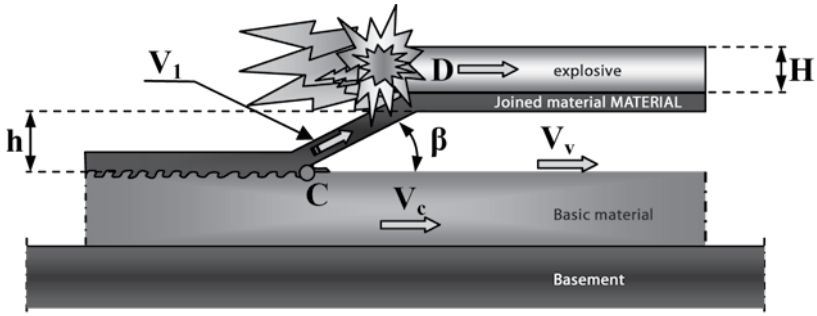


Fig. 1: Principle of explosive cladding

With aim of explosive cladding usually we can connect two layers, but in special cases joining tree layers is applied. As we can see in that pictures shape of joined places has wave shape. Explanation of this effect is shown in Fig. 2.

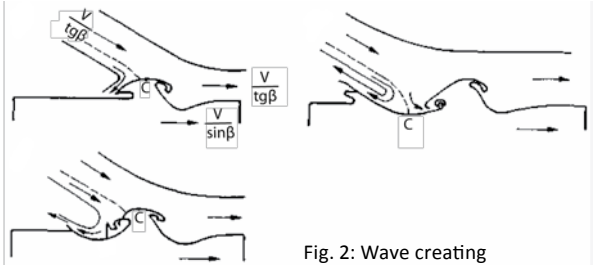


Fig. 2: Wave creating

## MATERIAL AND METHODS DESCRIPTION

Titanium and titanium alloys as progressive materials find many applications in industrial practice [1]. Production of so-called welding connectors is one of possible areas of explosive welding application. Generally, the welding connectors are metal composites having e.g. steel layer from one side and aluminium or aluminium alloy layer from the other. Three-layer composites in which carbon steel layer is separated from aluminium alloy layer by intermediate layer of pure aluminium are also very common. Another example of three-layer connectors is composites with intermediate layer made out of pure titanium. Such connectors are used in anode systems applied in electrolysis of aluminium as well as in shipbuilding industry for welding aluminium alloy structures to steel decks.

Application of titanium as intermediate layer enables connector to work in higher temperatures (up to 500°C). In that case, holding in a temperature of 500°C removes both strain hardening and hardening caused by phase transitions occurring in such specific bonding conditions [5,6]. It is especially essential for electrolysis of aluminium since the process can be performed at higher current intensities without misgivings about damage of anode system at bonding zone between aluminium rod and steel part of the anode. Moreover, using such type of connector the process of welding aluminium elements with steel ones can be done at higher welding parameters. Systems com-

posed of aluminium and steel layers only and those with intermediate layer made out of pure aluminium have limited application since temperature of aluminium – steel joint should not exceed 350°C.

Paper presents results of tests performed on laminar composite steel-titanium-aluminium manufactured by ZTW „Explomet". Preparation of experiment is shown in Fig. 3.

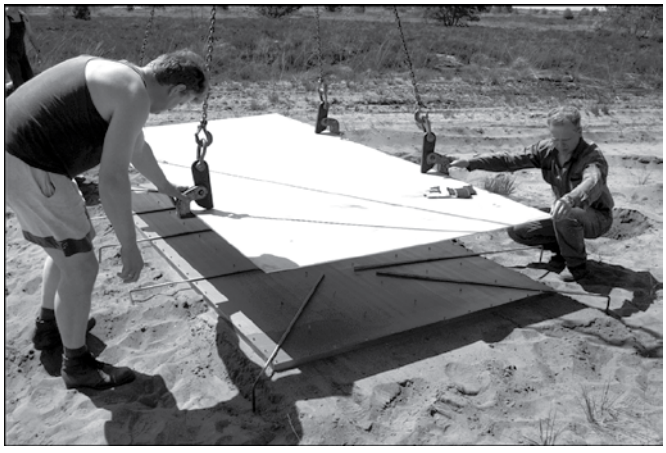

Fig. 3: Preparation of experiment

Trimetal plate having dimensions 480 x 500 x 55.5 mm was made up of ASME SB-516 Gr. 70 low-carbon steel plate, 40 mm thick and containing 0,12 ÷ 0,20% C, ASME SB-265 Gr.1 (>99.5% Ti) titanium plate 1.5 mm thick, and EN-573-3 EN AW Al199.7 aluminium plate 14 mm thick.

Explosive welding of all three materials was done simultaneously in the course of one shot after foregoing selection, calculation and testing of welding parameters such as type and amount of explosive, detonation velocity and structure of the system. Investigations presented in the paper refer to the trimetal of repeatedly good parameters ensured by appropriate welding parameters.

Investigations covered analysis of the wave, determination of quantitative portion of penetrations, analysis of macro-and microstructure, as well as change of hardening caused by explosive welding and subsequent heat treatment. Heat treatment consisted in heating up to 500°C, holding in such temperature for 24 hours and cooling down in surrounding air. Microstructure and micro hardness near of joint were investigated.

## RESULTS OF TEST AND THEIR ANALYSIS

The joint is characterised by parameters of the wave, amount of present penetrations and voids. The wave created at steel-titanium phase boundary has average length of about 2760 µm and height about 530 µm, whereas at titanium-aluminium phase boundary these values are accordingly 1570 µm and 310 µm (Fig. 4). Thus, the average wavelength and height on steel-titanium side are about 3 times bigger than those on steel-aluminium side.

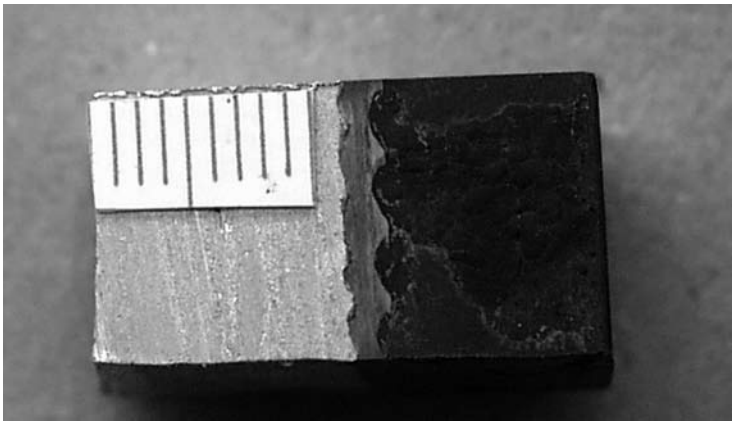

Fig. 4: Macroscopic analysis of the joint layers

Created wave deformed titanium intermediate layer in such a way that initial thickness of titanium plate changed locally from 1.5 mm to about 1 mm (between wave tops) and 2 mm (between wave hollows). Steel structure at bonding line consists of bainite-martensite regions, no voids or penetration were observed by macroscopic manner in obtained trimetal, generally (Fig. 5), in that kind of bonds such imperfections are disposed at the wave combs.

Changes of micro hardness in bonding zone were determined on cross-section at wave top and hollow (HV0,2), and at micro-areas containing penetrations or other substantial phase transitions (HV0,1), Hardness of steel near the phase boundary with titanium in non-heat treated joint is the biggest and amounts to about 310 HV0,2. The hardness decreases to about 225 HV0,2 as distance from contact line increases. Hardness of intermediate titanium layer varies in the range from about 215 to 230 HV0,2, whereas that of outside aluminium layer varies from about 40 to 50 $HV_{0.2}$. Applied heat treatment reduced hardness of steel, titanium and aluminium to about 200 HV0,2, 140 HV0,2 and 30 HV0,2 respectively.

In sample after heat treatment are occurred of essentials differences. Steel structure at bonding line consists of ferrite, pearlite and bainite-martensite regions. In the course of heat treatment, in bainite-martensite regions located closest to bonding line the phase transitions take place, which consists in cementite precipitation and diffusion of carbon towards steel-titanium boundary (decarbonising). As a result of these transitions the above-mentioned regions become fine-grained ferrite. The transitions are particularly active at wave combs where penetration layers and micro-voids occur (Fig. 6 and Fig. 7). As results from micro hardness tests, the biggest hardness belongs to penetrations bainite-martensite regions represent high value of hardness and the lowest hardness is that of titanium, nevertheless it is much higher than that of initial state before explosive welding (about 130 HV0.2). After heat treatment due to mentioned diffusive transitions the hardness of steel decreases while that of penetrations remains at very high level and achieve micro hardness of TiC (708 – 1034 HV0,1).

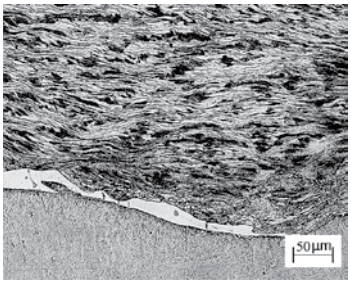


Fig. 5: Penetration layers occurred at sample without heat treatment (side steel-Ti)

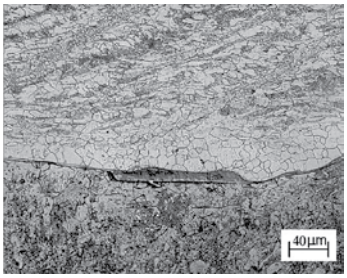


Fig. 6: Penetration layers occurred at sample after heat treatment (side steel-Ti)

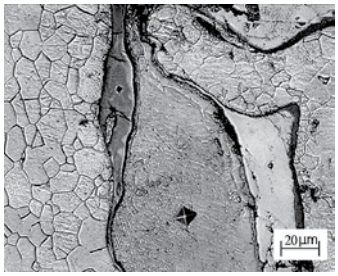


Fig. 7: Detail of penetration layers and decarbonising occurred at sample after heat treatment (side steel-Ti)

## CONCLUSIONS

The following conclusions can be drawn up:

- Contact surfaces between steel and titanium and aluminium are corrugated, there is small amount of penetrations and voids at bonding zone
- Aluminium and titanium sustain hardening throughout entire section while steel mainly at bonding vicinity
- hardening of aluminium and titanium results from dynamic plastic strain occurring in the course of explosive welding, hardening of steel comes from strain hardening and martensitic phase transitions
- heat treatment (annealing up to 500°C for 24 hours) removes hardening owing to recrystallization and decomposition of martensitic phases, decarbonising can appear near the Ti layer namely after high temperature and long time of annealing.

## ACKNOWLEDGEMENT

The work was co-financed by aim of projects of the Czech Republic Interredg IIIa, and sponsored project MSM 6198910015 and KONTAKT 42.

## Literature

Król S., Ptáček L., Hubáčková J., Lasek S., Čížek L., Gałka A., Szulc Z., Structure and properties of ruthenium coatings on titanium. In: Achievements in mechanical and materials engineering 2003, ps.539-542

Król S., Struktura i wlasności platerowanego wybuchovo zlasza typu stal 1H18N9T- stal 15HM, Archiwum Nauki o Materialach t.9, 1988, 2, p.131.

Król S., Szulc Z., Proc. VII Int. Conf. ”Spawanie w Energetyce”, Tatranska Lomnica-Matliare, 1996.

Król S., Welding International, 12, 5, 1991, p.944.

Szulc Z, Król S., Proc. Conf. ”GRE”, Bielsko-Biala, 1992.

Walczak W., Zgrzewanie wybuchowe metali, WNT, Warszawa1989.

# DEVELOPMENT OF NEW TESTING EQUIPMENT FOR INDUSTRIAL MACHINE DRIVES

Z. Češpíro, P. Mossóczy

**Abstract**

The article describes testing and development of tester for industrial machine drives or their parts. Testing equipment is designed for evaluation of kinematical, force and temperature quantities in short-term and long-term ranges. These devices are tested by repeated working cycles. Their parameter settings are possible to modify. LabVIEW development system is used for experiment control, data acquisition and data processing. The device is applied for testing of industrial brakes.

**Key words**

machine drives, experimental simulation, mechatronic systems, virtual instruments

Developed equipment is designed for assessment and testing of industrial machine drives or their parts. The force, kinematical, temperature and power service conditions are evaluated. Tested devices are loaded by various types of loading with different time slope of load spectrum in short-term, medium-term and long-term ranges. Test usually consists of series of repeated operating cycles. During these cycles the tested device is loaded by specific mode. The actual operating quantities – force, torque, speed, temperature are monitoring. Main purpose of tests is determination of base device operating parameters, description of device properties during long-term operating modes and verification of their dependability.

## BRAKE TESTER DESCRIPTION

The equipment was used to industrial disc brakes tests (Fig. 1).

These brakes are used as a regulating device to provide a constant speed. Another applying disc brakes as a safety run-out device is used. In the present case heat and frictional conditions of brake and their correlation are very significant. Testing brake

cycle consists of controlled engine run-up, short running with specified speed, run-out where motional energy is exploited inside the brake and stationary delay before next run-up. To simulate working load precise deceleration ramp function to engine speed control is used.

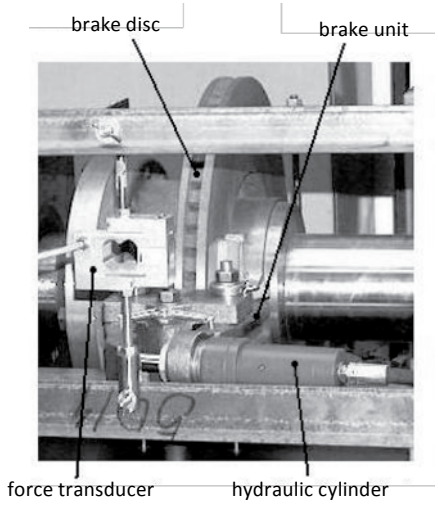


Fig. 1: Brake tester

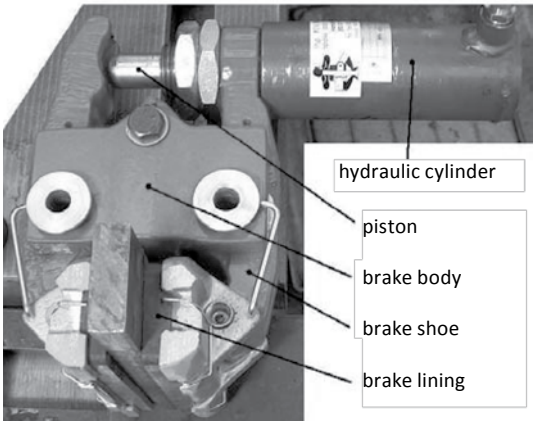


Fig. 2: Disc brake

Tested brake unit consists of brake body, hydraulic cylinder, pair of brake shoes running fit on pins and pair of brake linings (Fig. 2). Hydraulic piston presses the brake linings fixed on brake shoes to a brake disc. Testing equipment consists of main frame, special asynchronous motor with additional running diagnostics and independent cooling fan, brake unit with hydraulic cylinder, weight unit to brake balance located on auxiliary frame, gear coupling, shaft with brake disc supported on roller bearings (Fig. 3), hydraulic control unit with hydraulic gear pump, pressure oil accumulator and proportional control valve.

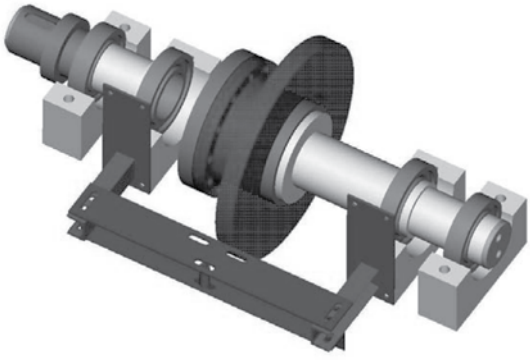

Fig. 3: Shaft with brake disc supported on roller bearings and auxiliary frame

## METHODOLOGY OF TESTER CONTROL

Testing process, running cycles control and saving measured data are provided by means of a personal computer (PC), which includes DAQ 6024E multifunction I/O board for PCI (DAQ card). The full development system with graphical language LabVIEW is used. The application is based on hierarchical and modular structures. The main application on top level calls independent subroutines with following tasks: tester control and configuration, data acquisition and processing, presentation of waveform of measurement. The main application sets number of testing cycles and working speed too. To change other parameters the configuration subroutine is called. The subroutine with tasks of tester control and data acquisition consists

of two main algorithms with parallel running and reciprocal synchronization. First algorithm uses data acquisition loop which calls DAQ library function to sample and transfer raw data into PC repeatedly. Online data processing and monitoring is used. Second algorithm is based on sequence, which launches tester control instructions in precise time interval. Sequence activates run-up and run-out of engine and controls duration of constant speed engine running and stationary delay before next run-up. Sequence initiates brake running and brake releasing too (Fig. 4). Time point of initiation of brake running and deceleration ramp function of engine must be synchronized precisely. Converter to control engine frequency is used. The application controls this converter by serial port with relevant communication protocol, precise vector control is used. Proportional valve to control brake activity is used. The electronic control card of proportional valve enables voltage or current control to be used. This application applies DAQ card voltage output. Monitoring of limit states is important part of subroutine. An abort of application by overrunning of these limits is running immediately.

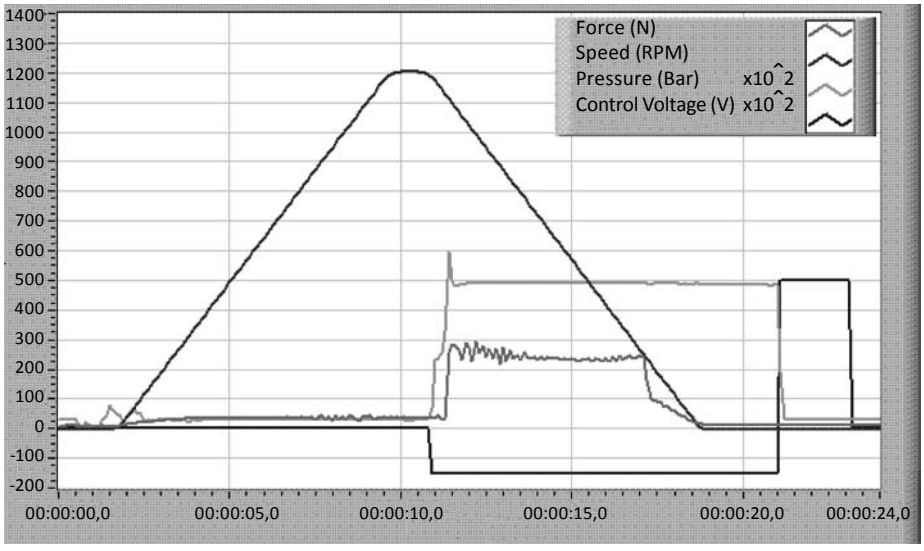


Fig. 4: Example of brake working cycle

## METHODOLOGY OF MACHINE DRIVES TESTING

Measurements in a short-term testing mode are focused on transient phenomenon for example damping in coupling, braking moment in brakes or deformation and stress dependences on motion or load. Because of these effects are very fast and short, the oscilloscope or DAQ card with high sampling rate has to be used. The data are record to memory of the oscilloscope or computer using data dependence on time. ASCII code data are ready to be transformed in graph. This method is acceptable for recording of analog signals. Measurements in a medium-term testing mode describe the effects in the start of service of drive. It means meas-

uring of temperature from starting service to steady service, definition of efficiency depending on degree of loading etc. Usually, the information of temperature of environment is recorded. Measurements in a long-term testing mode are focused on study of reliability, kinematic accuracy and other parameters during whole service life. We have to simulate loading for a long time. It means loading for thousands hours. It is necessary to design the optimal type of loading cycle. It usually consists of starting, running, braking, reversing, waiting etc. The most important parameters are temperature, torque moment, and speed. They have to be monitored to control the measure process.

## CONCLUSION

Designed tester provides possibilities to evaluate a large assortment of types of rotary machine drives. Modern universal testing, control and monitoring equipment to quick and exact evaluation of drives can be provided.

## Literature


Češpíro, Z., Mossóczy, P.: Development of Equipment for Testing of Drive Parts and their Monitoring Application of Work, Heat and Reliability Parameters. Acta Mechanica Slovaca, 1/2006.

Češpíro, Z., Chyský, J.: Metodika zkoušení kotoučových doběhových brzd. Výzkumná zpráva, ČVUT Praha, 2001.

Dynybyl, V., Češpíro, Z., Kanaval, J.: Experimental Evaluation of Starting and Braking Parameters of Braking Asynchronous Electric Motor. Workshop 2000, ČVUT Praha, 2000.

# THE ALUMINO-BOROSILICATE GLASS MELTS IN THE MGO-CAO-$AL_2O_3$-$B_2O_3$-$SIO_2$ SYSTEM – PHYSICOCHEMICAL PROPERTIES AND FOAM FORMATION

J. Kraxner, R. Klement, M. Liška

## Abstract

The high-temperature viscosity, density and surface tension of alumino-borosilicate melts as a function of temperature and glass composition were studied. The composition of studied glasses varies around the average composition (based on the average composition of major oxides in E-glass) in such a way, that in each case the molar % of one oxide is either increased or decreased and the molar ratios of other oxides in the system remain constant. The observed trends in glass melts properties (high temperature viscosity, density and surface tension) with composition are discussed in terms of possible structural changes of glass melts studied. The foam formation and its stability (kinetics of the foam collapse) have been studied as well.

## Key words

alumino-borosilicate glass melts, viscosity, density, surface tension, foam formation

Commercial E-glass melts must meet industry requirements (including ASTM specifications), [1] comply with environmental emission standards and have the lowest possible fibre forming temperature (or melt viscosity) that is consistent with a desired balance between material and energy costs. The melting behaviour of glasses depends on their viscosity-temperature relationship. Glass-melting furnace design and operation are largely determined by the temperature span within which melt viscosity allows successful melting, fining and conditioning of the glass. Therefore, the knowledge of glass viscosity as a function of temperature and glass composition is crucial for efficient glassmaking. Moreover, other properties at high temperature such as density and surface tension are important as well.

During the fusion of raw materials, a large quantity of gases is released from the batch by decomposition reactions. Gases such as $CO_2$, $O_2$, $SO_2$, CO and $H_2O$ vapor are released, and may result in primary foam, covering the batch blanket [2,3]. Secondary foam is formed in glass melting furnaces due to the gas bubbles, which are released

during the decomposition of refining agents dissolved in the glass melt [2,3]. This foam is entrapped at the glass free surface. Nevertheless, the viscosity and surface tension play important role in the ability of the glass melts to form a foam on the free surface of the glass melt and influence its stability.

In the present study high-temperature viscosity, density and surface tension as a function of temperature and glass composition are reported. The melting process of glass batches and foam formation (primary and pneumatic foams) on the surface of glass melts studied are reported as well. The composition of the glasses studied (Tab. 1) varies around the average composition in such a way, that in each case the molar % of one oxide is either increased or decreased and the molar ratios of other oxides in the system remain constant.

## EXPERIMENTAL

The glass batches were prepared by mixing of fine powdered $SiO_2$ (AFT, p.a.), $Al_2O_3$ (AFT, p.a.), $H_3BO_3$ (AFT, p.a.), MgO (AFT, p.a.), $CaCO_3$ (AFT, p.a.). The glasses were melted in Pt-10%Rh crucible in superkanthal furnace equipped with the Pt stirrer at temperature of 1500°C for four-five hours in ambient atmosphere. The molten glasses were poured into a metal mould and the glass blocks were then annealed at temperature of approximately 500°C for 1 hour and finally slowly cooled down to room temperature (RT). The high-temperature viscosity of melts was determined by falling sphere method. The densities of glasses at RT and glass melts were measured by Archimedes method, dual weighting of glass in air and in distilled water or glass melts, respectively. The surface tension was measured using the sessile drop (a stationary drop on a substrate) arrangement. The non-wetting substrate (glassy carbon – Sigradur G) in inert atmosphere (N2) was used. The melting process proceeding in an optical quartz cuvette, placed in the specially designed furnace, was monitored by digital camera and the images were recorded and treated using software for imaging analysis (LUCIA, LIM Prague). The pneumatic foam was generated by bubbling of glass melt with air through the Pt-capilary. This methodology enables us to observe and study individual stages of the glass melting process, e.g. sintering, melting, glass melt refining, foam formation.

Tab. 1: The composition of glasses studied, based on the average composition of major oxides in E-glass and the step Δ of change in the composition of each oxide.

| Oxide | Average composition (mol. %) | Δ (mol. %) |
|---|---|---|
| MgO | 2.44 | ± 2.44 |
| CaO | 26.49 | ± 3.00 |
| $B_2O_3$ | 4.59 | ± 2.00 |
| $Al_2O_3$ | 8.96 | ± 3.00 |
| $SiO_2$ | 57.52 | ± 4.00 |

## RESULTS AND DISCUSSION

The selected results of high temperature viscosity and density measurements are shown on Fig. 1. The surface tension of the glass melts studied is summarized in Tab. 2. In Fig. 1 and Tab. 2, the symbol "Ave." denotes the glass melt with average composition (see Tab. 1), the symbols e.g. MgO+ and MgO- denote the glass melts with either increased or decreased amount of MgO oxide in the glass melts, but the molar ratios of other oxides in the melt remain constant. The same is valid for the other oxides in the system MgO-CaO-$Al_2O_3$-$B_2O_3$-$SiO_2$.

Tab. 2: Surface tension of the glass melts studied measured at temperature correspondingto log 2.

| Glass | $\gamma$ [mN.m$^{-1}$] | Temperature [K] for log($\eta$ /dPa.s) = 2 |
|---|---|---|
| **AVE.** | 417 ± 2 | 1639 |
| **MgO+** | 388 ± 2 | 1599 |
| **MgO-** | 320 ± 2 | 1683 |
| **CaO+** | 350 ± 2 | 1609 |
| **CaO-** | 339 ± 2 | 1684 |
| **$B_2O_3$+** | 386 ± 2 | 1629 |
| **$B_2O_3$-** | 350 ± 2 | 1672 |
| **$Al_2O_3$+** | 354 ± 2 | 1646 |
| **$Al_2O_3$-** | 334 ± 2 | 1620 |
| **$SiO_2$+** | 345 ± 2 | 1673 |
| **$SiO_2$-** | 383 ± 2 | 1632 |

The melt viscosity vs. temperature was described by the Arrhenius-like equation (also known as Andrade´s equation):

$$\log(\eta/\mathrm{dPa.s}) = A + B/T \qquad (1)$$

where A, and B are constants routinely determined by the regression analysis, and T is the thermodynamic temperature. The temperature independent viscous flow activation energy, Ea, was calculated by eqn. 2:

$$E_a = \left(\frac{\partial(\ln\eta)}{\partial(1/T)}\right)_p R = \ln(10)RB = 2.303RB \qquad (2)$$

where R is the molar gas constant.

As clearly seen from Fig. 1, the glass modifiers (MgO and CaO), decrease the melt viscosity, over the whole temperature range measured, with their increasing amount in the glass melt, compared to glass melt with average composition. Reversely, the decreased amount of glass modifiers leads to the increase of glass melt viscosity, over the whole temperature range.

For the glass former oxide $SiO_2$ it was found, that increasing amount of $SiO_2$ in glass increases viscosity of the glass melt, however, decreasing amount of $SiO_2$ leads to the moderate decrease of glass melt viscosity, over the whole temperature range.

On the other hand, increasing amount of the other glass former, $B_2O_3$, leads to the moderate decrease of the glass melt viscosity, and decreased amount of $B_2O_3$ to increase of glass melt viscosity, over the

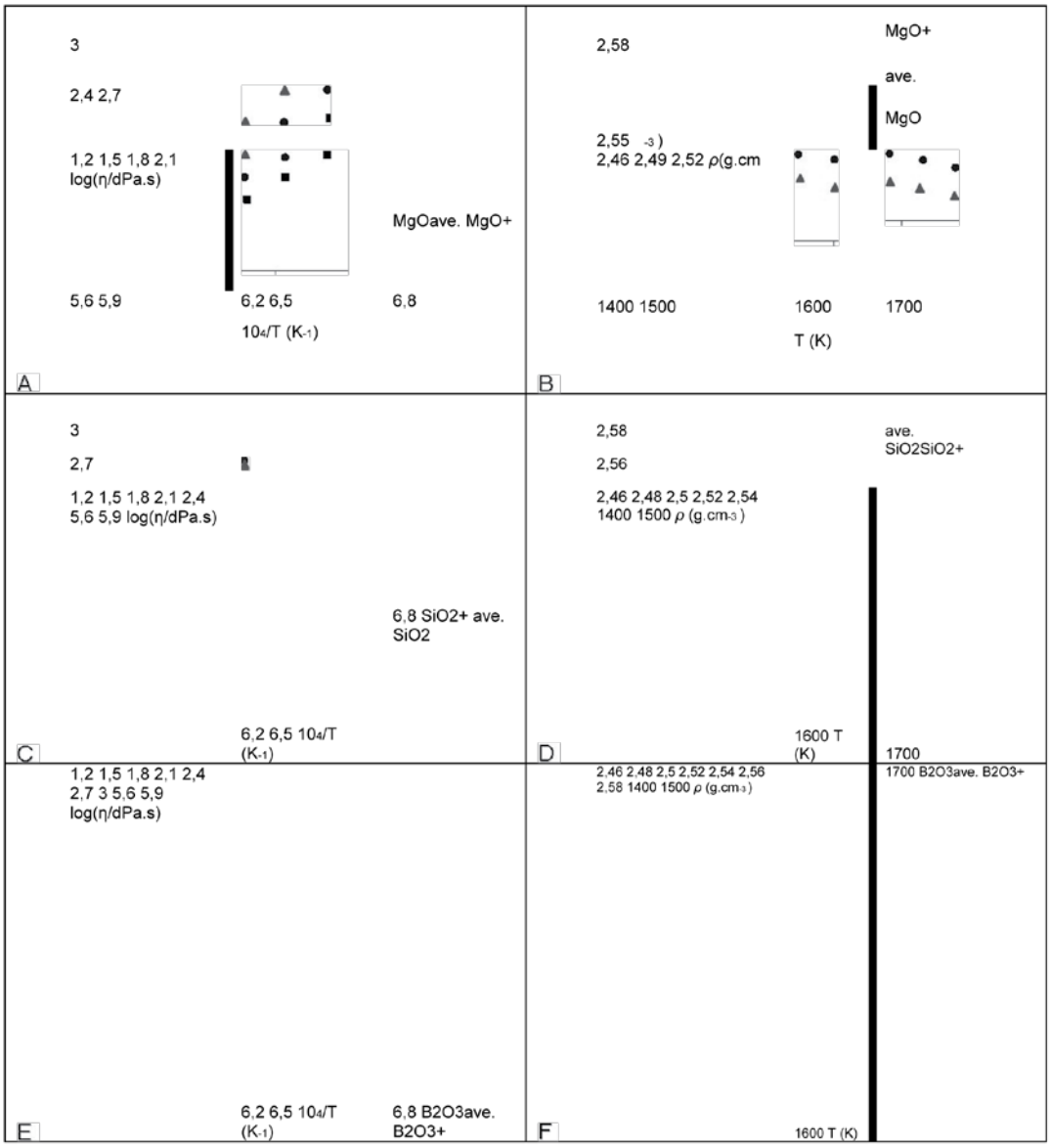


Fig. 1: High temperature viscosity and density of the glass melts as a function of temperature: A) viscosity and B) density for melts Ave., MgO+ and MgO-; C) viscosity and D) density for melts Ave., $SiO_2$+ and $SiO_2$-; E) viscosity and F) density for the melts Ave., $B_2O_3$+ and $B_2O_3$-.

whole temperature range measured. The change in the composition of $Al_2O_3$ only slightly affects the viscosity of the glass melt compared to the melt denoted as Ave. Similar trends were observed for high temperature density of glass melts.

The observed trends in glass melts properties (high temperature viscosity, density) with composition can be discussed in terms of possible structural changes of glass melts studied. It was found, that viscosity of the glass melts decreases with decreasing value

of the $SiO_2$/RO ratio; RO represents the sum of molar % of MgO+CaO oxides. This can be attributed to the greater extent of structural network depolymerization. The addition of the former oxide $B_2O_3$, generally decreases the glass melt viscosity. The temperature independent activation energy of the viscous flow, Ea, was found to be in the range 250 – 260 $kJ.mol^{-1}$ for all glass melts studied.

The surface tension of the glass melts studied was determined by sessile drop method. The surface tension was calculated using the drop profile recorded by digital camera and known value of density of the glass melt at given temperature. The values of surface tension are summarised in Tab. 2. It was found that the surface tension is most significantly affected by the change of the amount of MgO oxide in the glass melts.

Unfortunately, only very little amount of primary foam was formed during the melting process of the batches and the same observation was found for pneumatic foam generated by bubbling of glass melts with air. This fact unable us to study the stability of the foam formed and the kinetics of foam collapse.

## ACKNOWLEDGEMENT

This work was supported by Agency for Promotion Research and Development under the contract APVV-20-P06405, by the Slovak Grant Agency for Science under the grant VEGA 1/3578/06, and by the university grant No.16/2006.

## Literature

ASTM Standard D 578-00, Annual Book of Standards, American Society for Testing and Materials, Conshohocken, Pa., Mar. 10, 2000.
Beerkens, R.G.C., Van Der Schaaf, J., J. Am. Ceram. Soc., 89, 2006, 24.
Fedorov, A.G., Pilon, L., J. Non-Cryst. Solids, 311, 2002, 154.

# INFLUENCE OF TEMPERATURE CHANGES DURING LABORATORY TESTS OF ROCK PERMEABILITY

J. Šperl, J. Trčková

## Abstract

Laboratory determination of porous material permeability is more problematic the less permeable the tested material. The permeability test of less permeable materials is of long duration, lasting up to several days. Therefore, many factors affect the results of the test. The impact of water temperature changes, flowing through a material sample during the test, was studied. The viscosity of water varies with temperature change, also affecting changes in the differential pressure. Less permeable rock samples were tested under laboratory conditions. It was found that water temperature changes of about 1.5 °C affected measured permeability of rock samples with a permeability coefficient of less than 10-11. Therefore, to obtain faultless results of permeability tests, it is possible to place a permeability instrument in the room with constant temperature.

An instrument for permeability measurement having a high technological standard enables measurement of material during a constant hydraulic incline according to the ČSN, CEN ISO/TS 17892-11 was used.

## Key words

permeability, laboratory test, rock samples, temperature changes

Permeability is the ability of solid porous materials (e.g. soils and rocks) to leak a fluid or gas through its pores and cavities. Permeability is one of the basic properties of solid materials. On the basis of the known permeability, possible influences of water on an engineering construction are considered. Knowledge of the permeability is necessary at water leakages, at the structural foundation in order to evaluate affluent to a foundation pit, in terms of the design of waterproofing of buildings. The permeability is also a very important indicator for the utilization of various kinds of the rocks [2].

To determine permeability, various methods can be applied, which differ in the medium used. In the case when the fluid that passes through the porous material is water, permeability can be expressed by the coefficient of conductivity k ($m.s^{-1}$), which means a discharge velocity of water flow in a rock under the action of a unit hydraulic gradient

$$k = \frac{Q.l}{A.h.t} \ (m.s^{-1}),$$

where

*Q* volume of water flows through the specimen during time t
*l* is the height of the tested specimen (the length of the path that water has to flow through the rock)
*A* is the cross-section of the specimen
*h* is the difference in the water pressure levels
*t* is the period of measurement.

## APPARATUS FOR COEFFICIENTCONDUCTIVITY DETERMINATION

An apparatus of a high technological standard was used, enabling permeability measurements on fully saturated specimens of soil and rock under constant hydraulic incline [1]. The apparatus is composed of a panel with measuring and regulation elements, containing a horizontal burette that enables exact measurements of the water volume flowing through during saturation as well as during permeability measurement; vertical (overflow) burette which enables exact measurements of the volume of water flowing through the sample during measurement of permeability; differential micro-manometer for level difference measurement; piston hand pump for pulling in/pulling away the membrane on the measured specimen in the cell during handling before and after measuring; needle valve, which opens the water intake from pressurised vessels to the panel; and regulation cocks. A permeability cell of a membrane type is also placed. In the cell, it is possible to place cylindrical specimens from 25 mm to 50 mm in height, and a diameter up to 50 mm. Lower and upper bases of the cell have an outlet for pressure difference monitoring.

Sources of saturated pressure and differential pressure are two interconnected pressurised cylindrical vessels with heavy pistons. Pistons are exchangeable and their mass is graded to allow setting the required pressure by combining the pistons. Hydrostatic cell pressure is created by a separated pressure tank, located several metres above the level of the other parts of the apparatus. Location of this tank guarantees that the cell (confining) pressure is always higher than the pressure at the bottom base of the cell. Hydrostatic cell pressure is constant; it is not measured, and presses only the membrane to the cylindrical surface of a specimen. This prevents water passing around the specimen during test. The apparatus has three sensors for water temperature monitoring. Measured values are recorded by a central programmable measuring device. Communication with the central measuring device and their following processing is made from operating system Windows [4].

## METHOD OF PERMEABILITY MEASUREMENT – DESCRIPTION OF SELECTED TESTS

Laboratory testing of permeability is carried out according to the Czech version of the technical specification CEN ISO/TS 17892-

11:2004. The above mentioned specification has the status of the Czech standard [3].

The test consists of two basic phases after placing the specimen in a cell: (i) saturation of specimen (ii) running permeability test. While putting the specimen in the cell in which the permeability is measured and taking it out, a moderate de-pressurisation is applied, pulling the membrane from a specimen towards the cell shell. The saturation of the specimen, and also the permeability measurement, is carried out when an overpressure to the cell is applied, which presses the membrane to the cylindrical surface of a tested specimen.

The saturation of the specimen is carried out at the same level of the saturated pressure that is 150kPa for all tested specimens. The rock saturation phase is completed when the water volume going into and out of the specimen is equal. At the same time, it is desirable that the value of differential pressure is maintained at the level at which the laminar flow in the system still occurs.

Tab. 1: Conductivity coefficient of tested specimens

| | Specimen (types of rocks, locality ) | Coefficient of conductivity $k_{10}$ ($m.s^{-1}$) |
|---|---|---|
| PERMEABLE ROCKS | Sandstone Záměl | 1,72 E-06 |
| | Sandstone Hořice | 2,30 E-06 |
| | Sandstone Hamr | 2,82 E-06 |
| | Sandstone Kamenné Žehrovice | 3,34 E-06 |
| | Sandstone sample 282 | 6,02 E-06 |
| | Sandstone Podhradí | 7,33 E-06 |
| | Sandstone Úpice | 1,16 E-07 |
| | Sandstone sample 20 | 1,51 E-07 |
| | Sandstone Zámostí | 5,69 E-07 |
| | Sandstone Kocbeře | 9,25 E-07 |
| | Sandstone Jitrava | 7,07 E-08 |
| VERY FEW PERMEABLE ROCKS | Arenaceous marl sample 7 | 1,67 E-09 |
| | Marlite Vraňany | 2,87E-09 |
| | Sandstone Zdislava | 4,55 E-09 |
| | Limestone Úvaly | 5,34 E-09 |
| | Corundum 1100 | 1,24 E-10 |
| | Granite | 1,54 E-10 |
| | Granite Potůčky-Podlesí | 2,21 E-10 |
| | Clayey limestone Litoměřice | 2,82 E-10 |
| | Marlite Litoměřice | 8,08 E-10 |
| | Basalt Boží Dar | 5,15 E-11 |
| | Limestone Koněprusy | 5,67 E-11 |

During the permeability measurement, the quantity of water going through the specimen is measured. The course of the test is observed on the computer monitor. The test of permeability is finished when time dependence of flowing water quantity is constant.

## TESTED SPECIMENS

Laboratory tests were conducted on a rock specimen of cylindrical shape drilled from compact rock materials with following proportions – height of tested specimen: 50 mm; basis diameter of tested specimen: 50 mm. Based on rock permeability, tested specimens were divided into two categories. Very few permeable rocks (rock permeability varies from $10^{-8}$ to $10^{-11}$) and permeable rocks (rock permeability varies from $10^{-8}$ to $10^{-4}$).

In total, 22 various rocks were tested (Tab. 1). Coefficient of conductivity was predominantly determined as the arithmetic average of two to five rock specimen tests.

## INFLUENCE OF TEMPERATURE ON COURSE OF ROCK PERMEABILITY MEASURING

As stated in chapter 4, rock specimens were divided into two categories.

The first group of rock specimens represents permeable rocks (sandstones). In the case of these specimens, experiments last from 30 to 60 minutes. During this time period, temperature does not change. Therefore, water kinetic viscosity is constant and has no effect on the volume of water leaking through the rock specimen during measurement. The curve of rock permeability is increasing dynamically (Fig. 1 and 2).

Second group of rock specimens represents very few permeable rocks. The permeability measurement experiments of these specimens usually last up to several days - data are recorded by computer-readable device with scan (time) period around 10-15 minutes. It allows observation of changes in water volume leaking through the specimen for long time periods and its dependency on temperature. Despite the fact that temperature changes during the tests were small (did not exceed 2ºC), it is obvious that the volume of water leaking through the specimen, which is very small, is strongly influenced by this fact. Water kinetic viscosity is declining, so water amount is decreasing, too. We can clearly see the effect of these changes in Fig. 3 and 4.

Fig. 3 shows rock permeability and temperature addiction of artificial corundum. Whole laboratory test had lasted 3 days 2 hours and 15 minutes. We can identify that for the first 22 hours, the cumulative volume of water leaking through the specimen was increasing. At the end of this period, temperature started to rise, and as consequence, the amount of water going through the specimen decreased. This state had lasted for 5.5 hours when the temperature became to fall again, and as consequence, the amount of water going through the specimen increased, etc.

Fig. 4 shows the same “sinusoidal curve” as in the previously described laboratory test, in this case for basaltic rocks. Generally, when the temperature decreases, the curve of permeability of rock specimen increases, whereas when the temperature increases, permeability decreases.

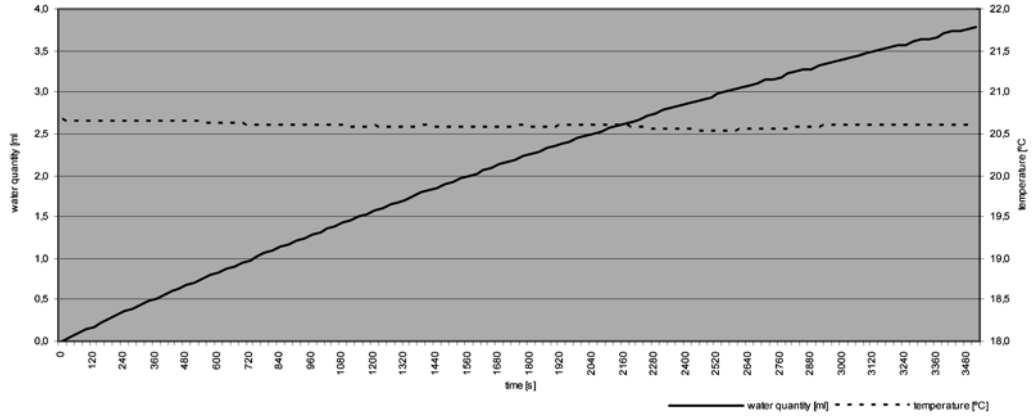


Fig. 1: Graph of rock permeability and temperature addiction - sandstones

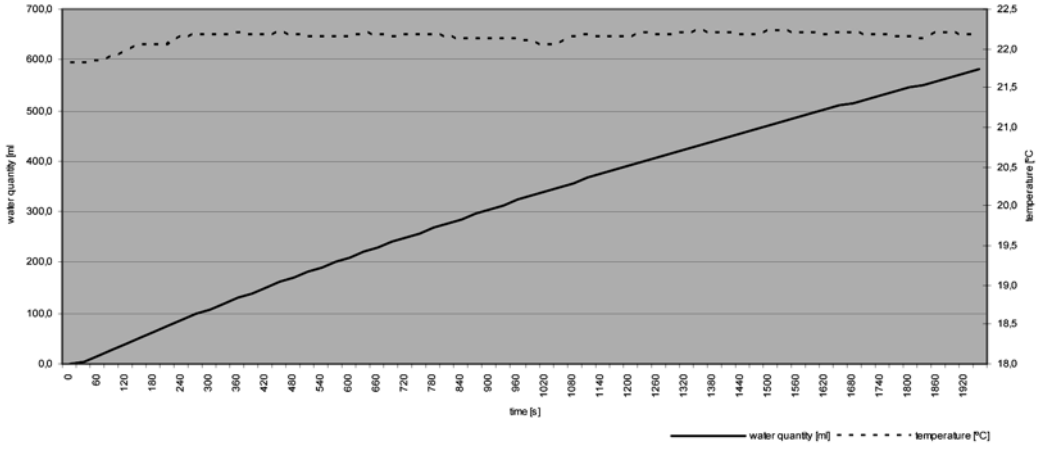


Fig. 2: Graph of rock permeability and temperature addiction - braun sandstones

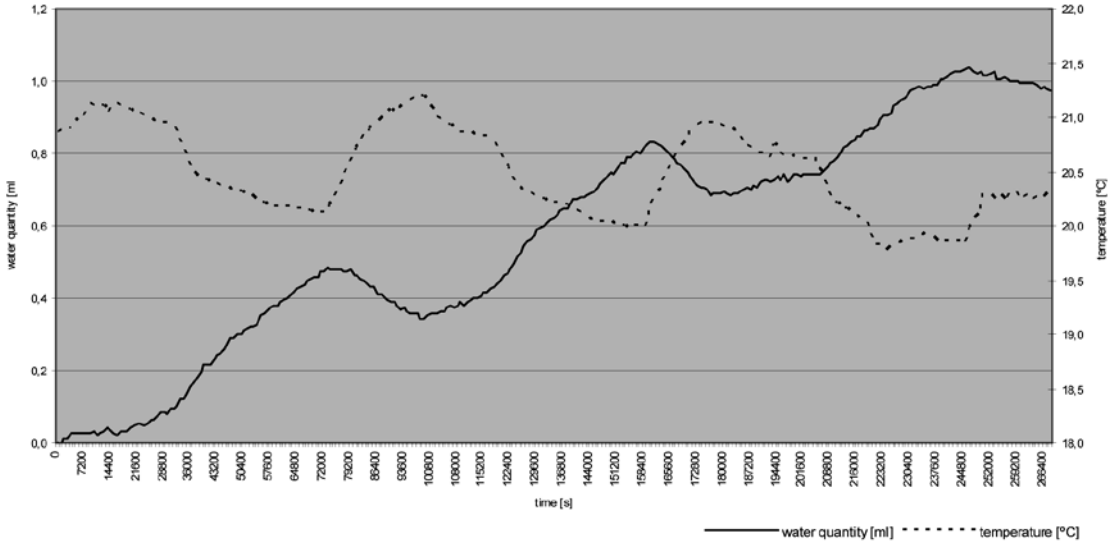


Fig. 2: Graph of rock permeability and temperature addiction - artificial corundum

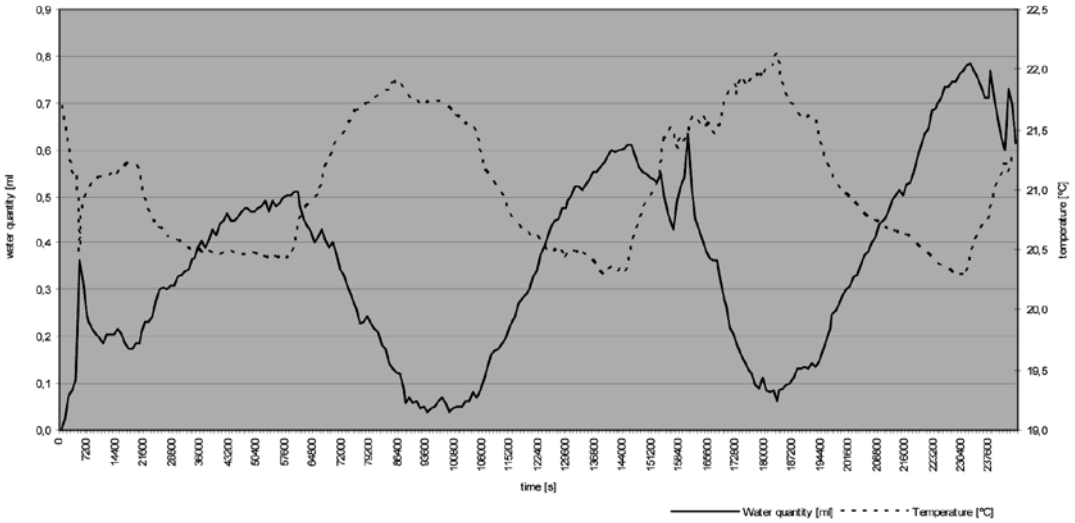

Fig. 2: Graph of rock permeability and temperature addiction - basalts

## CONCLUSION

According to the Czech version of the Technical specification CEN ISO/TS 17892-11:2004, it is recommended to keep temperature not exceeding a range of 2ºC during the laboratory tests of rock permeability. During our laboratory tests, we realized that even values of this temperature range strongly affect the amount of water leaking through the specimen. Despite the fact that temperature changes have only a small influence on the total values of the permeability coefficient, it is strongly recommended to carry out permeability measurements in an air-conditioned room with constant temperature.

## ACKNOWLEDGEMENT

This paper was partly supported by Grant Agency of the Academy of Sciences of the Czech Republic, grant project No. IAA2119402, entitled: “Stress and deformation states in structures and structural elements using coupled modelling”.

## Literature

Brůha, P., Březina, M., Straková, J., Trčková, J., Živor, R.: Laboratory apparatus to measure porous material permeability. Acta Montana IRSM AS CR, series A 18 (121), 75-79, 2001.

Christensen, B.J., Mason, T.O., Jennings, H.M.: Comparison of measured and calculed permeabilities for hardened cement pastes. Cement and Concrete Research, Vol.26, No.9, 1325-1334, 1996.

ČSN, CEN ISO/TS 17892-11 Geotechnical investigation and testing – Laboratory testing of soils – part 11: Determination of permeability by constant and falling head, 2005.

Straková, J.,Trčková, J., Živor, R.: Permeability measurement of natural construction materials. Stavební obzor, Vol.10, No.11, 307-310, 2002

# INDIRECT VERIFICATION OF IMPACT TESTING MACHINES ACCORDING TO EUROPEAN AND AMERICAN STANDARDS

R. Holušová , J. Borkala

## Abstract

Charpy impact testing machines can be verified by direct verification based on measuring physical and geometrical properties and also by indirect verification. Both methods are recommended according to the European and also American Standards. Indirect verification by means of Standard Reference Test Specimens provides global examination of Impact Testing Machine and using of this methode is acc. to ASTM E 23 necessary.

## Key words

indirect verification of impact testing machines

### Two Methods of Verification

Charpy impact testing belongs to the testing of basic mechanical properties. Every impact testing machine shall be annually verified. According to the European and also American Standards there are two methods of verification:

- **the direct method,** which consists of inspecting the machine to ensure that requirements of the physical and geometrical properties are met to
- **the indirect method** – global verification using Standards Reference Test Specimens.

## VERIFICATION OF IMPACT TESTING MACHINES ACCORDING TO EUROPIAN STANDARD

### Direct Verification

The direct method shall be used, firstly, when the machine is being installed or repaired and, secondly, if the indirect method gives an incorrect result in order to find the reason for it.

Direct verification relates to machine framework, pendulum, framework position, test piece support and anvils, position of centre of percussion, energy indicator, initial potential energy, indicated energy error, friction losses and impact velocity.

Although this direct method shall be used in cases thereinbefore, most of testing laboratories in the Czech Republic verify their impact testing machines only by this direct method.

## Indirect Verification

Principle of this verification there is determination of the energy absorbed by breaking of Charpy V reference test pieces from batches whose breaking energy is known.

The total absorbed energy consists of:

- the energy required to break the test pieces
- the internal energy losses of the pendulum impact testing machine

The energy losses are due to:

- air resistance and bearing friction and friction due to drag of the pointer
- foundation impacts and vibration of the framework

The Charpy V reference test specimens is possible to order e.g. in IRMM (Institute for Reference Materials and Measurement ) in Brussel (Fig. 1).

EUROPEAN COMMISSION

**COMMUNITY BUREAU OF REFERENCE - BCR**

**CERTIFIED REFERENCE MATERIAL**

CERTIFICATE OF MEASUREMENT

Batch AP

**C R M 013** N°. 22

**IMPACT TOUGHNESS OF V-NOTCH CHARPY SPECIMENS**
**(energy level 30 J nominal)**

| Impact energy at 20 ± 2 °C | Certified value (1) | Uncertainty (2) |
|---|---|---|
| According to EN 10045-2: 1992 [According to ISO 148-3: 1998] | 29.4 J | 0.7 J |

(1) This is the mean impact energy for the 5 specimens delivered in one set.
(2) Estimated expanded uncertainty as defined in the Guide to the Expression of Uncertainty in Measurement, ISO, 1995 (coverage factor k=2).

**DESCRIPTION OF THE MATERIAL**

A unit comprises of five specimens which must be broken successively in the machine to verify. The specimens are packed in protective oil and cleaning must be done as recommended.

**INSTRUCTIONS FOR USE**

Specimens should be kept in their original packing until they have to be used. Special attention is drawn to cleaning. The following procedure is recommended:

1. Wipe excess of oil from the specimens with cellulose paper.
2. Immerse the specimens in a clean bath of degreasing solvent for about five minutes.
3. Wipe the specimens with cellulose paper and allow to dry in still air.
4. Before testing, allow the specimens to equilibrate to laboratory temperature for about 24 hours.

After cleaning the user must avoid touching the specimens with the fingers (wear clean gloves). Vigourous cleaning methods (such as making use of brushes or ultrasonic cleaning) going beyond the steps described above should be avoided, as this can result in obtaining erroneous data. At energies above 100 Joule it is equally important that after each strike both the anvils and the striking edge are cleaned with a soft tissue.

NB: When expert advice is required on the impact testing machines, the user should contact the Local Accreditation Body.

Brussels, 19 March 2001
Revised August 2003

BCR
for certified true copy

Fig. 1: Example of the Belgian Certificate

Indirect verification shall be carried out for a least two levels of energy. For impact testing machines within the actual range 300 J there is better to use three levels. These three levels of energy shall be uniformly distributed in the range of application.

Five test pieces are broken for each level, the test being carried out at a temperature of (20±2)°C.

In Tab. 1 there is shown an example of the values in indirect verification of impact testing machine.

The evaluation is made by the Czech Metrology Institute.

It stands to reson from the table Tab. 1 that indirect verification according to EN 10 045-2 is not exceedingly strict.

## VERIFICATION OF IMPACT TESTING MACHINES ACCORDING TO AMERICAN STANDARD

### Direct Verification

Complete direct verification shall be carried out at installation of new impact testing machine and than immediately after replacing parts that may affect the measured energy, after making repairs or adjustments, after they have been moved, or whenever there is reason to doubt the accuracy of results, without regards to the time interval.

Otherwise only some items shall be inspected annually – specimens supports, anvils, and striker.

### Indirect Verification

Indirect verification requires the testing of specimens with certified values to verify the accuracy of Charpy impact machines.

Tab.1: Example of indirect verification

| CRM No. | Certified value [J] | Measured values [J] | Everage value [J] | Repeatability [J] | | Repeatability [J] | | Uncertainty k=2 [J] |
|---|---|---|---|---|---|---|---|---|
| | | | | $E_{max}$-$E_{min}$ allowed | $E_{max}$-$E_{min}$ achieved | $\bar{E}$ -E allowed | $\bar{E}$ -E achieved | |
| AP No.20 | 29,4 | 31,7<br>30,0<br>31,7<br>31,0<br>30,5 | 31,0 | 6,0 | 1,7 | ±4,0 | +1,6 | 1,4 |
| N No.7 | 60,6 | 60,2<br>59,8<br>61,6<br>60,0<br>60,5 | 60,4 | 9,1 | 1,8 | ±6,1 | -0,2 | 1,5 |
| G No.35 | 159,4 | 168,0<br>164,0<br>178,0<br>162,0<br>178,0 | 170,0 | 23,9 | 16,0 | ±15,9 | +10,6 | 12,5 |

Verification specimens with certified values are produced at low (13 to 20J), high (88 to136J) and super-high (176 to 244 J) energy levels. To meet the verification requirements , the average value determined for a set of verification specimens at each energy level tested shall correspond to the certified values of verification specimens within 1,4 J or 5,0 %, whichever is greater.

Verification specimens are available from the NIST (National Institute of Standards and Technology) through the Standard Reference Materials Program.

National Institute of Standards and Technology
Materials Reliability Division
325 Broadway
Boulder, CO 80305-3328

Facility: Vitkovice Testing Center, Pohranicni 584/142
Ostrava, Viktovice 706 02 Czech Republic

Machine Manufacturer: Amsler Serial Number: 76

Test Date: 6/20/2006

| SERIES NUMBER | CLIENT VALUES | | | | | UNITS | AVERAGE (J) | | VARIANCE | STATUS |
|---|---|---|---|---|---|---|---|---|---|---|
| | 1 | 2 | 3 | 4 | 5 | | CLIENT | NIST | | |
| Low LL-98 | 16.0 | 16.8 | 16.2 | 16.1 | | J | 16.3 | 15.9 | 0.4 J | Pass |
| High HH-98 | 114.0 | 105.5 | 105.0 | 107.0 | | J | 107.9 | 105.7 | 2.1% | Pass |
| Super High SH-TDS | 228.0 | 227.0 | 220.0 | 224.0 | 230.0 | J | 225.8 | 222.8 | 1.4% | Pass |

Allowable Variance is 1.4 J or 5%, whichever is greater (ASTM Standard E 23)
NT = NOT TESTED

Fig. 2: Part of verification Certificate from NIST with the values

It is not easy to product material for SRM specimens. Two materials are currently used to make the specimens for indirect verification of Charpy impact machines to E 23 specification. A 4340 steel is used to make specimens for low- and high-energy levels. A type T-200 maraging steel is used to make specimens for the super-high-energy level.

In these steels, the hardness, impact energy, and strength are interrelated. Since hardness correlates to impact energy and is a more convenient property to measure during processing, it is used as the initial process control.

The low-energy specimens are typically heat-treated to attain a room-temperature hardness HRC of 45, which corresponds to a Charpy impact energy near 16 J at – 40°C. The high-energy specimens are typically heat-treated to attain a room temperature HRC of 32, which corresponds to a Charpy impact energy near 100 J at – 40°C, the super- high-energy specimens are typically heat-treated to attain a room temperature HRC of 30, which corresponds to a Charpy impact energy near 220 J at room temperature (Fig. 2).

Acceptability of verification specimens is based on combination of three criteria:

- dimensional tolerances of specimens
- mean and standard deviation of impact energy
- the direction in which the specimens leave the machine during impact testing

Indirect verification according ASTM standard is very strict and clever. Just matching the reference energy is not sufficient to confirm that the machine is fully satisfactory. For example, worn anvils can combine with high-friction bearings to compensate for each other and produce an artificially correct value during the verification test. These are called compensating errors. Unfortunately, these errors compensate only over part of the range, so the machine produces generally inaccurate values. The post-fracture examination of the NIST standardized verification specimens is a good way to identify such effect. Therefore, the NIST specimens come with a questionnaire with critical questions about the machine and the test procedure.

All specimens are examined and compared to the data on questionnaire before a formal response is sent to the customers.

## CONCLUSION

Although indirect verification shall be used according to European and American Standards, indirect verification is not in common use in Europe, the fabrication of samples has not long tradition. In 1990, four master batches of 30, 60, 80 and 120 J nominal energy were certified by BCR. Certification methodology is based on between-laboratory testing and uncertainties .

Indirect verification according to ASTM E 23 is necessary part of general verification for a long time and that is why American method is more elaborated. Charpy impact machine without this indirect verification is not acceptable for testing according to ASME Code and ASTM Standards.

## Literature

Vigliotti, D. P., Siewert, T. A., Mc Covan, C. N.: Installing, Maintaining, and Verifying Your Charpy Impact Machine, NIST, 2000.

Annual Book of ASTM Standards, Section 3 – Metals Test Methods and Analytical Procedures, Volume 03.01 Metals – mechanical Testing; Elevated and Low-Temperature Tests; Metallography, 2003.

European Commission: BCR Information – Reference Materials, The Certification of Two New Master Batches of V-Notch Charpy Impact Toughness Specimens in accordance with EN 10045-2:1992

# ANALYSIS OF SLOPE EFFECT AND GEOMETRY OF GLULAM PITCHED CAMBERED BEAMS – ADVISES FOR THEIR DESIGN AND PRACTICAL APPLICATION

A. Bjelanović, V. Pavlić, V. Rajčić

## Abstract

This paper represents a part of diploma work[2] in the scope of glued laminated girders of special geometry. It also shows results of previous research[1, 3] engaged in the field of timber (material and structural design) and FEM. The main subjects of our interest are glulam pitched-cambered beams the form of whom is aesthetically very impressive. However, an unsuitable form, e.g. inappropriate slope, due to the span and radius of curvature of the apex zone, could incite very serious problems in practice and jeopardize a safety of the whole structure. Wood is an anisotropic material whose tensile strength perpendicular on grains is far below the rest of its material properties. Therefore, we must deal very seriously with the safety of the curvature zone of girder, where these stresses appear. EC5 makes some simplifications that are acceptable enough in engineering practice. We tried to compare the results obtained using different codes and FEA.

## Key words

glulam pitched cambered main girders, curvature, structural safety and practical design, comparison of European codes, analysis of parametrically prepared FE models

From the aspect of architecture, pitched cambered glulam beams of great intrados curvature are aesthetically very attractive and desirable shapes of main girders. On the other hand, from structural and technological view, the complex geometry of those girders is a potential limit to their economic application. A big intrados curvature in the ridge zone, non linear distribution of stresses along the cross section's width, and both a complex state of stresses caused by girders' geometry and anisotropy of wood as a material make it necessary to handle carefully the calculation of those girders. As for their mechanical resistance and stability, the study of tensile strength perpendicular to grains intensified by curvature is of enormous significance. The bearing capacity of wood in regard to tension perpendicular to grains is exceptionally low and varies significantly from its other mechanical properties. It is therefore hard

to optimize the dimensions of those girders according to this criterion as its other characteristic cross-sections are not enough used. Such a problem can be avoided in different ways: local strengthening of the curved area, the construction of ridge girders of reduced static height (rounded ridge) or the construction of girders in couples instead of uneconomic increase of the single girder's height. Much better solutions relate to the geometry's rationalization (the slope of the flat girder's part of the axis, the raise of the curved area radius and the variation of the static height – full or reduced, modifying or constant girder's height as well) in relation to the span. The paper advocates such an approach, and the results lead to the summary of guidelines for a practical usage. As the basis for an investigation new European norms were taken, EN 1995:2004-1-1. We compared the results with those of the calculation according to pre-norms, DIN ENV 1995:2000-1-1.

The proofs for mechanical strength and stability of the characteristic section x-x relevant for the stability control differ in the norm and pre-norm. The FE 2D and 3D girders' models are parametrically prepared as well, undergoing the static analysis and global stability analysis (buckling) in order to look at the impact of simplification which leads to the introduction of norms into the calculation. The expressions for dimensioning (norms) by a series of coefficients transform the non linear stress distribution with respect to the height of the cross- section into a linear one, and a complex stress state transforms into bending stresses. FE analysis done in COSMOS/M package reflects a real state of stresses and deformations. Therefore, we wanted to investigate whether, and to which extent are the practical proofs of mechanical strength and stability on the side of safety. The paper addresses just a small part of research deals with investigations in the field of limits of suitable geometry on certain spans.

## DESCRIPTION OF METHODS INCLUDED IN RESEARCH

The constants in the calculation are as follows:

Mechanical properties (strength, stiffness and density modules) of comparable classes of laminated wood with high bearing capacity and of 1st serviceability class – BS 28H (DIN ENV 1052:2000) made from structural timber S13, and GL 28H (EN 1995:2004) made from structural timber C30 class.

The 5,0 m distance of main girders and characteristic load of 1,25kN/m$^2$ as a short - term action. The total value of the constant action has been estimated to be 0,7kN/m$^2$.

Symmetric load of main girders (the wind impact omitted – asymmetric impact).

The application of programme packages and the approach to the calculation (parametrically conducted analyses):

Programme package MATCHAD 13 for the proofs of mechanical strength and girders' stability. The girders are modelled parametrically (seven input parameters are: intrados and extrados slope angles,$\alpha$ and $\beta$, their divergence, y, L girder span, chord length on the Cin intrados dependent on the radius and central curvature angle, affecting the volume of the curved zone, then cross-section dimensions – the height on the girder's bearing, ha and the width, b). The alteration of stresses and the estimation of the cross - section's bearing capacity (satisfying or not) result from varying the input parameters.

The Excel programme package has been used for limiting the input parameters values ($\alpha,\beta,\gamma,L,C_{in}$, $h_a$, b) so as to evaluate the girder's rationality. The assessment of rationality (dependence of mechanical strength and girder's stability on geometry). With regard to limitations of the study scope (samples' number, simplified analysis only for symmetric actions, etc.), rationality assessment for the glulam girders of highly curved intrados can be considered as a design «guideline».
The COSMOS/M programme package has been used for MKE analysis of parametrically modelled girders (the same input parameters) undergoing the same analysis and repetitive calculations. The package is used to introduce the possibility of comparing results with those obtained by the calculations and application of expressions for dimensioning (EN, ENV).

## PARAMETRIC DESIGN PROCEDURE OBTAINED IN ACCORDANCE WITH EC5 CODES

The calculation's procedure diagram shows the ways in which the girder's calculation and the analysis of design's rationality along with the construction of related girders were conducted. The paper presents the required stages to dimension accurately and rationally the girder (pitched camber and/or curved girder of high intrados curvature). The girders are simple static schemes (freely leaning beams), and the curvature is in the limits of $2 \le R / h_{ap} < 10$, tj. $0,1 \le h / R < 0,5$. The design of these girders is technologically far more complex as the axis in the ridge zone is designed by inserting the short radius curve. The number of phases and the mode of gluing the plates affect the static height and the bearing capacity in the ridge zone (full or reduced cross-section of pitched cambered girders). However, the height in the ridge exceeds 3,0 m of the production hindrances (the limit value is here restricted to 2,5 m). The curved area's volume limitation is 2/3 from the total girder volume. The biggest transversal slope of these girders limits to the value $\le 25^0$. There is also an additional limitation related to the value difference $\alpha - \beta \le 10^0$ for the pitched cambered girders, the cross-section height of whom changes due to varied slope angles of extrados ($\alpha$) and intrados ($\beta$). Such a condition results from the fact that the plates are, generally laid parallel with one of the girder's generatrices. Therefore, the effect of oblique slashed edge appears on the opposite generatrix. The unsuitable effect that oblique weakening has on the values of components of complex stress state gets modified by limiting the generatrices' slope difference.

In the practice, the shapes of laminated pitched cambered girders of curved intrados can be constructed so that their static cross-section height in the ridge zone gets reduced (fitted apex), whereas the constant remains (concentric curvature). In the zone where the girder's axes the straight line's height of girder's cross-section can be either changeable or constant. Due to the reduction of static height in the ridge zone they are treated as curved girders.

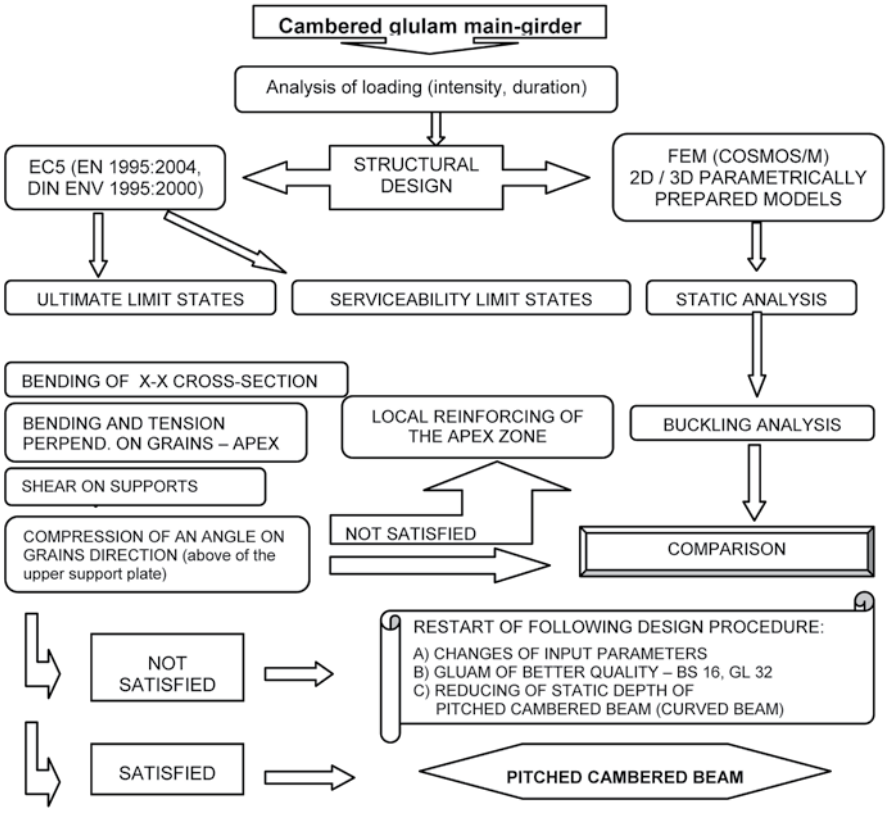


Fig. 1: Flow-chart of design procedure and parametric analysis

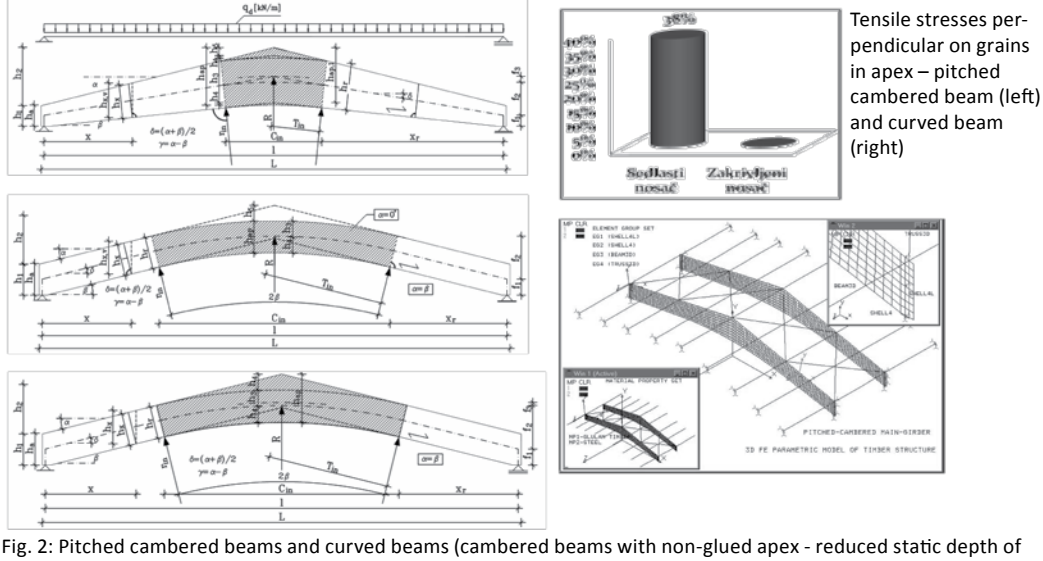

Tensile stresses perpendicular on grains in apex – pitched cambered beam (left) and curved beam (right)

Fig. 2: Pitched cambered beams and curved beams (cambered beams with non-glued apex - reduced static depth of cross-section) on left. 3D parametrically prepared FE models – SHELL4L (girder), BEAM 3D (purline),TRUSS 3D (bracing diagonals) and PLATE FE (just for upper support plates) on right.

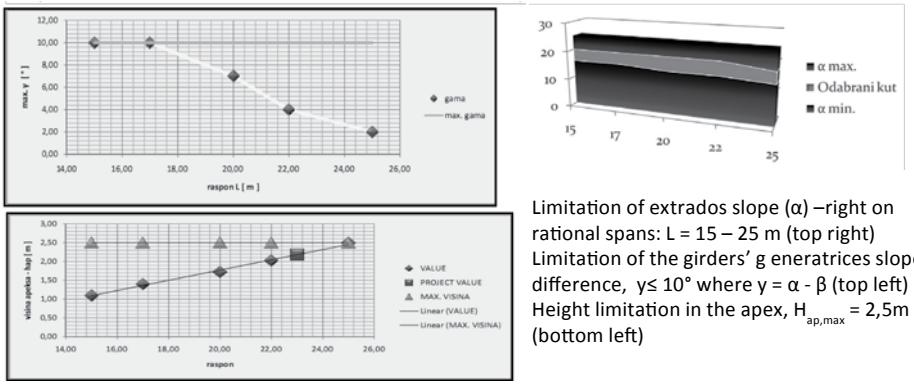


Limitation of extrados slope (α) –right on rational spans: L = 15 – 25 m (top right)
Limitation of the girders' g eneratrices slope difference, y≤ 10° where y = α - β (top left)
Height limitation in the apex, $H_{ap,max}$ = 2,5m (bottom left)

Fig. 3: Input parameters, values of limitations and obtained results

The comparison of the design according to ENV and EN does not show major differences in the utilisation and safety. The difference in the value of partial coefficients for material ($y_M$ = 1,25 according to EN or $y_M$ = 1,3 according to DIN ENV is negligible). As far as the calculations are concerned, the only difference relates to the treatment of the characteristic cross-section x–x on the girder's flat part, where the difference in the cross-section utilisation (bending and stability), in the notched extrados is 30% – 36%, and the calculation according to EN 1995-1-1:2004 (eq. 1, 2) is on the safety side in relation to DIN ENV 1995-1-1:2000 (eq. 3,4). The difference in the utilization of cross-section x– x on the lower flat intrados is little and amounts some 15%. The comparison with FEA shows that the impact of longitudinal force (visible in FE models) for the girders with a usual bearing combination (unmovable and movable) is negligible. Therefore, the simplifications applied in the norms are practice related and acceptable from the engineering point of view, in laboratory research and the theory of anisotropic plates. The cross-section positions x – x with the highest stress from bending, comparing FEA and EC5 are not the same.

$$\sigma_{m,d,\gamma} = \frac{M_{x-x,d}}{W_{x-x}} \le k_{m,\gamma} \cdot f_{m,d} \quad (1)$$

$$k_{m,\gamma} = \frac{1}{\sqrt{1 + \left(\frac{f_{m,d}}{1{,}5 f_{v,d}} \cdot tg\gamma\right)^2 + \left(\frac{f_{m,d}}{f_{c,90,d}} \cdot tg^2\gamma\right)^2}} \quad (2)$$

$$\sigma_{m,d,\gamma} = (1 - 4\,tg^2\gamma) \cdot \frac{M_{x-x,d}}{W_{x-x}} \le k_{m,\gamma} \cdot f_{m,d} \quad (3)$$

$$k_{m,\gamma} = \frac{1}{\frac{f_{m,d}}{f_{c,90,d}} \cdot sin^2\gamma + cos^2\gamma} \quad (4)$$

## CONCLUSION

For the above described cambered beams the vital bearing capacity proof for tension perpendicular to grains in the apex, especially when there are greater slopes. By connecting the stress lengths perpendicular to grains obtained from EC5 and FEM we get to the difference in the distribution and values of the results, which is confirmed by the connection with the slope. Both design methods include conforming to the stress increase trend, but not with the stress magnitude. The design of pitched cambered girders is not rational on the L > 25m spans. The better solutions present the curved girders (L < 30m) or the full replacement of static system.

## Literature

Bjelanović, A., Rajčić, V.: Timber structures accordingly European norms, HSN and Faculty of Civil Eng. in Zagreb, Zagreb, 2005. (republished, 2007.)
Pavlić, V.: Glulam cambered beams – parametrically prepared analysis of rationality based on EC5 and FEM, diploma work, Faculty of Civil Eng. in Rijeka, Rijeka, 2007.

# INVESTIGATION OF RESIDUAL STRESSES PRODUCED BY MACHINING OF STEEL STRUCTURE PARTS

J. Běhal, N. Ganev, M. Černý

## Abstract

Residual stresses in technological samples with different procedures of surface machining are investigated. Test specimens were made from high-strength steels (L-ROL, L-CM3, 300M and Ph13-8Mo), chosen according to demands of the aerospace industry. The influence of lathe-turning, grinding and shot peening is evaluated on the basis of the experimental results. Optimizations of cutting conditions are recommended. Residual stresses on the specimens' surface were analyzed by means of X-ray diffraction technique using CrKα radiation. The spacing of atomic planes {211} α-Fe was measured and residual stress values were subsequently calculated from the obtained lattice deformations.

## Key words

residual stress, X-ray diffraction, steel specimen, machining

Increased use of high strength steel enables to reduce structure weight. However, these modern materials are sensitive to heat treatment and the surface quality. Reduction of detrimental tensile residual stresses improves properties of structure parts significantly. Shot peening provides industrial components with an enhanced fatigue life and with an increased fatigue limit under cyclic loading. This is a result of generation of compressive residual stresses in the near-surface regions of the components.

However, there is not a simple relationship between the parameters of machining and the residual stresses induced in the surface layers of treated materials [1-3]. Final results of surface treatment depend on its parameters, and on properties of treated material including microstructure and crystallographic structure. This kind of surface treatment causes complex microstructural changes, which can be monitored in a non-destructive mode using X-ray diffraction methods. Therefore reliable methods of experimental stress analysis have to be ap-

plied for control of the resultant state of residual stresses. X-ray diffraction method is one of the most developed and efficient analytical tools for evaluation of stress fields in polycrystalline materials.

The "one tilt" X-ray diffraction technique without any reference material [1] was applied for residual stress determination, Fig. 1. A position sensitive detector (imaging plate) was used for detection the {211} diffraction of the CrKα-radiation. The stress values were calculated from the observed lattice deformations using the X-ray elastic constant. All the measurements were performed with a cylindrical collimator 2 mm of diameter. Experimental error of evaluated stresses does not exceed 40 MPa [2].

## TESTED SPECIMENS

The steels examined in this study were commercial L-ROL (Fe-0.32C-1.0Mn-1.1Si-1.0Cr-0.3Ni-0.25Cu), L-CM3 (Fe-0.26C-0.65Mn-0.27Si-1.1Cr-0.20Mo-0.30Ni-0.25Cu), 300M (Fe-0.41C-0.76Mn-1.67Si-0.73Cr-1.8Ni-0.38Mo-0.04Al-0.005Sn-0.001Ti-0.05V-0.11Cu) and PH13-8Mo (Fe-0.03C-13Cr-8Ni-2.5Mo-1.2Al). These materials are often used for high loaded structure parts of airframe. Material samples were heat-treated according to standard specifications. Cylindrical specimens were 45 mm in diameter. The girth was machined by the lathe-turning and grinding. In the both cases, the influence of afterwards shot peening treatment was analysed. Parameters of machining process, such as cutting speed and horizontal shift, as well as shot-peening intensity, were optimized.

## RESULTS

The results of residual stress on turned surface versus cutting conditions are shown in Figs 1-2 for axial and transversal direction. Values in the both directions should be considered together, because of shared cutting conditions. However, for the purpose of machining parameter optimisation they are simply analysed separately.

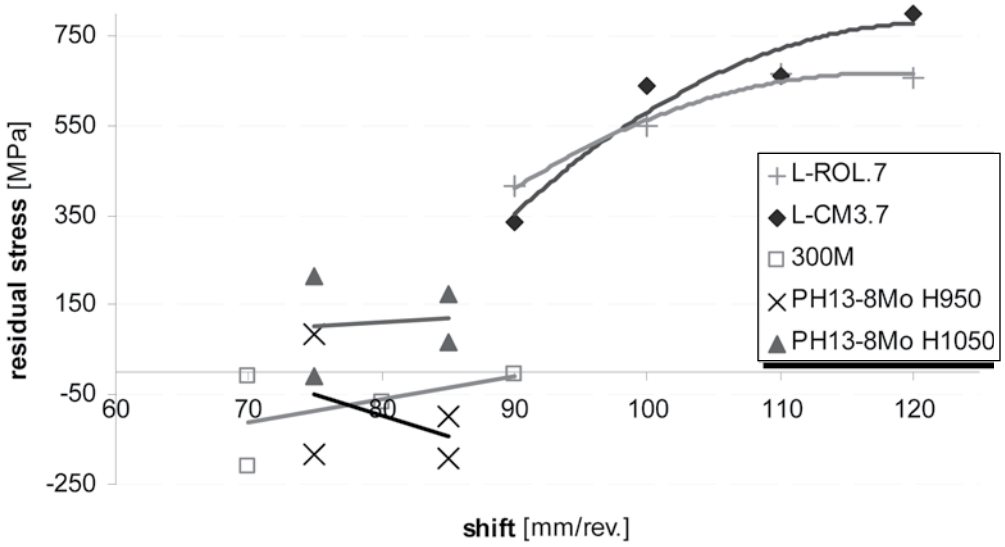


Fig. 1: Residual stresses in axial direction on the turned surface.

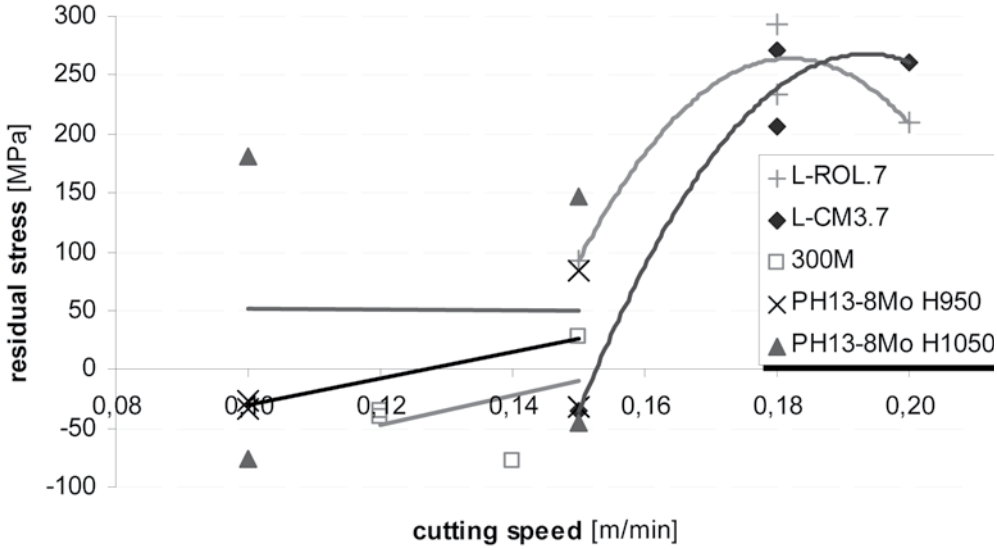


Fig. 2: Residual stresses in transversal direction on the turned surface.

In the Fig. 3, the results of grinded surface are presented for both directions. Parameters of grinding were given by rigid context as limit temperature of specimen surface depended on the material and grinding wheel structure.

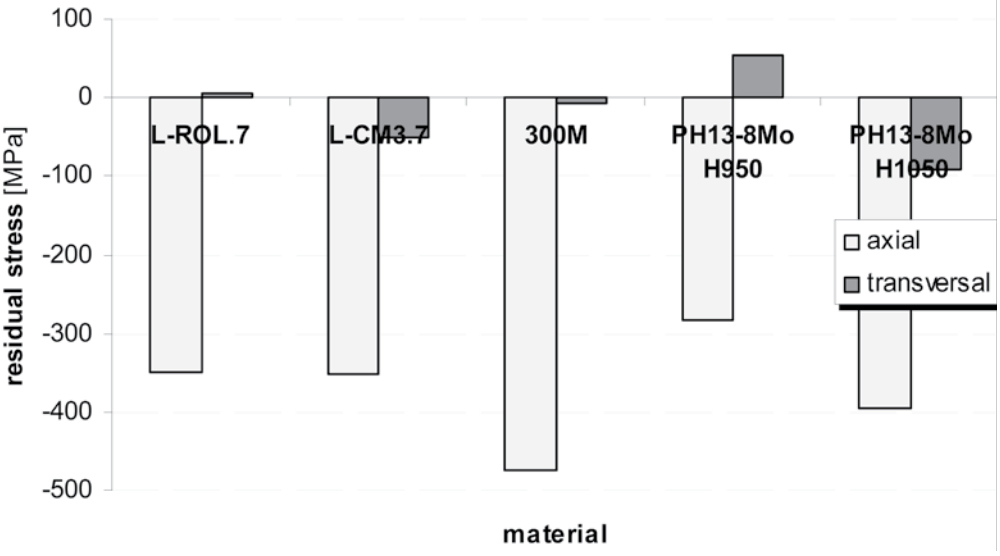


Fig. 3: Residual stresses in axial and transversal direction on the grinded surface.

The afterwards shot peening give the uniformity resulted in the compressive residual stress. For each material, the values of surface stress are approximately of the same level in the tested range of shot-peening intensity (see Fig. 4). The depth of affected layer corresponds to the peening intensity [3] and lower surface value of the compressive stress for the higher shot-peening intensity is probably given by surface plastic deformation and dislocation of maximum residual stress to the deeper layer.

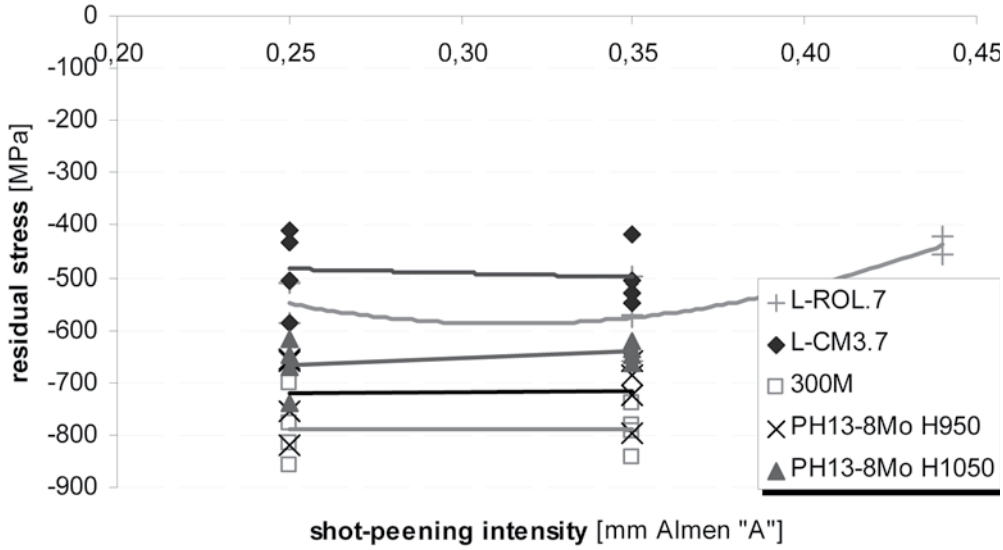


Fig. 4: Residual stresses versus shot-peening intensity.

## CONCLUSION

Residual stresses in steel specimens were examined by means of X-ray diffraction. This way the parameters of machining process may be optimised and an improvement of shot peening application may be considered. Such experimental investigations are important for the industry applications, because the effective processing is the key to meet the economic requirements.

For more detailed examination it will be useful to perform measurements of the depth distribution of residual stresses beneath the sample surface. For this purpose the removing of the material layer by electrolytic polishing is applied. The removal of surface layers gives rise to a partial relaxation of the residual stresses and observed values have to be corrected for this effect. However, the number of experimentally measured points grows rapidly.

Changes of the crystallographic planes' spacing can be measured and converted into a residual stress. Diffraction can be accomplished with X-rays, which provide information from the surface and bulk of a material, respectively. Measurement at many locations within the specimen and its surface leads to maps of residual stresses of the real structure part. These stress maps are used for model validation and prediction of structure life. X-ray diffraction provides a powerful means of very accurate determination of microstructure, strains and mechanical behaviour in a way, which is not possible with other experimental techniques.

## ACKNOWLEDGEMENT

This study was supported by the Ministry of Industry and Trade of the Czech Republic, project no. FT-TA/026.

## Literature

Kraus I., Ganev N.: Residual Stress and Stress Gradients, In: Industrial Applications of X-ray Diffraction, Ed. F.H.Chung and D.K.Smith, Marcel Dekker, Inc., New York-Basel, 2000, pp. 793-811.

Ganev, N. et al.: X-ray study of residual stress distribution in surface layers of shot-peened steels, Proceedings of 23rd Danubia-Adria Symposium 2006, Podbanské, Slovakia, ISBN 80-8070-589-5, pp. 17-19

Běhal, J.: Life Extension of Fatigued Steel Specimens by Shot Peening, Czech Aerospace Proceedings 2/2004, Prague, Czech Republic, ISSN 1211-877X pp. 5-6.

Alexander Dubček
University of Trenčín
ISSN 1337-6047